Liquid-phase Exfoliated GeSe Nanoflakes for Photoelectrochemical-type Photodetectors and Photoelectrochemical Water Splitting

Gabriele Bianca,[†,ᵗ,‡] Marilena I. Zappia, [§,ᵻ,‡] Sebastiano Bellani,[§,*] Zdeněk Sofer,[ᴵᴵ] Michele Serri,[†] Leyla Najafi,[§] Reinier Oropesa-Nuñez,[§,ǂ] Beatriz Martín-García,[†,#] Tomáš Hartman,[ᴵᴵ] Luca Leoncino,[ᵀ] David Sedmidubský,[ᴵᴵ] Vittorio Pellegrini,[†,§] Gennaro Chiarello,[ᵻ] and Francesco Bonaccorso[†,§,*]

[†]Graphene Labs, Istituto Italiano di Tecnologia, via Morego 30, 16163, Genova, Italy

[§]BeDimensional Spa., via Albisola 121, 16163 Genova, Italy

[ᵗ]Dipartimento di Chimica e Chimica Industriale, Università degli Studi di Genova, via Dodecaneso 31, 16146 Genoa, Italy

[ᴵᴵ]Department of Inorganic Chemistry, University of Chemistry and Technology Prague, Technická 5, 166 28 Prague 6, Czech Republic

[ᵀ]Electron Microscopy Facility, Istituto Italiano di Tecnologia, via Morego 30, 16163 Genova, Italy

[ᵻ]Department of Physics, University of Calabria, Via P. Bucci cubo 31/C 87036, Rende (CS), Italy

[ǂ]Department of Material Science and Engineering, Uppsala University, Box 534, 75121 Uppsala, Sweden

[#]CIC nanoGUNE, 20018 Donostia-San Sebastian, Basque, Spain

KEYWORDS: germanium selenide (GeSe), photocatalysts, water splitting, two-dimensional materials, hydrogen evolution reaction (HER), oxygen evolution reaction (OER)

ABSTRACT: Photoelectrochemical (PEC) systems represent powerful tools to convert the electromagnetic radiation into chemical fuels and electricity. In this context, two-dimensional (2D) materials are attracting a huge interest as potential advanced photo(electro)catalysts and, recently, 2D group-IVA metal monochalcogenides have been theoretically predicted to be water splitting photocatalysts. In this work, we use density functional theory (DFT) calculations to theoretically investigate the photocatalytic activity of single-/few-layer GeSe nanoflakes for both the hydrogen evolution reaction (HER) and the oxygen evolution reaction (OER) in pH conditions ranging from 0 to 14. Our simulations show that GeSe nanoflakes with different thickness can be mixed in form of nanoporous films to act as nanoscale tandem systems, in which the flakes, depending on their thickness, can operate as HER- and/or OER photocatalysts. Based on theoretical predictions, we report the first experimental characterization of the photo(electro)catalytic activity of single-/few-layer GeSe flakes in different aqueous media, ranging from acidic to alkaline solutions: 0.5 M H_2SO_4 (pH 0.3), 1 M KCl (pH 6.5), 1 M KOH (pH 14). The films of the GeSe nanoflakes are fabricated by spray coating GeSe nanoflakes dispersion in 2-propanol obtained through liquid-phase exfoliation of synthesized orthorhombic (*Pnma*) GeSe bulk crystals. The PEC properties of the GeSe nanoflakes are used to design PEC-type photodetectors, reaching responsivity up to 0.32 AW^{-1} (external quantum efficiency of 86.3%) under 455 nm excitation wavelength in acidic electrolyte. The obtained performances are superior to those of several self-powered and low-voltage solution-processed photodetectors, approaching the one of self-powered commercial UV–Vis photodetectors. The obtained results inspire the use of 2D GeSe in proof-of-concept water photoelectrolysis cells.

INTRODUCTION

The conversion of light energy into chemical fuels and electricity through photoelectrochemical (PEC) cells represents a powerful strategy for sustainable fuel and chemical generation,[1–4] environmental remediation (*i.e.*, pollutant degradation),[5–7] advanced analytical systems (*i.e.*, chemical sensors) for environmental[8,9] and biological monitoring,[9–11] as well as innovative self-powered photodetectors.[12,13] In particular, PEC water splitting is envisioned to produce molecular hydrogen (H_2),[14,15] seen as ideal energy carrier for the storage and distribution of solar energy in the so-called "Hydrogen economy".[16,17] Alongside, aqueous PEC cells, including water splitting ones, are emerging for the development of cheap, easily-fabricated, environmentally friendly self-powered photodetectors with high spectral responsivity (> tens of mA W^{-1} for UV-visible spectral region),[12,18–20] fast response (in the order of tens of ms)[12,19,21] and satisfactory sensitivity (typically in the order of 10).[12,19,22] To achieve efficient PEC systems, it is necessary to develop photocatalytic materials that efficiently absorb light in the desired spectral range (UV/visible for energy conversion systems)[23], creating free charge carriers with

suitable energies to accomplish the targeted oxidation-reduction (redox) reactions before they recombine.[23–25]

In this context, two-dimensional (2D) materials, including either single- and few-layer flake forms, are attracting utmost interest as potential advanced photo(electro)catalysts.[26–29] Such attention mainly relies on their large surface-to-volume ratio, which guarantees that the charge carriers, *i.e.*, electrons and holes, are directly photogenerated at the interface with the electrolyte, in which redox reactions take place before their recombination.[26–29] Both theoretical and experimental works investigated the photocatalytic water splitting properties of graphene derivatives,[30–33] as well as other 2D materials, including graphitic carbon nitrides,[34–36] transition metal dichalcogenides (*e.g.*, MoS_2,[37,38] WS_2[39,40] and ReS_2[41,42]) transition metal oxides[43] (*e.g.*, $H^+/K_4Nb_6O_{17}$,[44] $TBA^+/Ca_2Nb_3O_{10}$[45]), (functionalized) mono-elemental materials (*e.g.*, phosphorene[46–49] germanane,[50] silicane,[50]), MXenes,[51] group-IVB metal nitride halides,[52] group-IIB metal monochalcogenides (*e.g.*, ZnSe,[53,54]) and group-IIIA metal monochalcogenides[55–57] (*e.g.*, GaSe[58] and InSe,[59,60]).

Recently, 2D group-IVA metal monochalcogenides (MX, M = Si, Ge, Sn, Pb; X = S, Se, Te), namely SiS, SiSe, SiTe, GeS, GeSe, GeTe, SnS and SnSe, have been theoretically predicted to be low-cost and environmentally friendly water splitting photocatalysts.[61–68] However, the field evaluation of their photo(electro)catalytic properties is still missing, pointing out the need of experimental trials and validation. Theoretical studies revealed that their monolayer form is stable both in the phosphorene-derived distorted NaCl-type structure ("black-phase structure", space group: $Pmn2_1$),[69–76] and the *Pma2* structure.[69,77] However, a large variety of polymorphisms, including blue-phosphorene-like *Cmcm* structure,[72,75,76,78–82] cubic polymorph,[83] $Fm\bar{3}m$ structure,[84,85] $P2_1ca$ structure[81,86–88] and *P4/nmm*,[70] have been synthetized at high temperature or pressure,[83,89] and/or predicted to be metastable.[70,87,88] Importantly, each material polymorphs shows distinctive optoelectronic properties,[90] which can be further tuned by strain engineering,[76,91–94] thus creating a material platform for novel nanoelectronics. Among the plethora of 2D group-IV metal monochalcogenides, GeSe polymorphs have been deeply investigated for application in several fields, including photovoltaic,[95–98] photodetectors,[82,99–105] (tunnel) field-effect transistors,[106–109] spintronic,[110,111] piezoelectric actuators[88],[112] and ferroelectric devices,[113] and energy storage systems,[114,115,116,117] beyond to be proposed as water splitting photo(electro)catalysts.[61,62,68,93] Density functional theory (DFT) calculations revealed that its cleavage energy from the corresponding orthorhombic bulk structure is around 0.45 J m^{-2},[62] which is similar or slightly superior to those calculated for other 2D materials, including graphene (0.3–0.4 J m^{-2},[118,119] experimental value: 0.37 J m^{-2}),[120] several transition metal dichalcogenides[121] (*e.g.*, MoS_2, 0.29 J m^{-2}),[121] group-V elemental materials (*e.g.*, phosphorene, 03–0.4 J m^{-2})[122,123] and several group-IIIA metal monochalcogenides (*e.g.*, GaSe, 0.29 J m^{-2}).[57,58] These results suggest that 2D GeSe can be easily produced through the exfoliation of its bulk counterpart, including either micromechanical cleavage-based exfoliation[124–126] or scalable liquid-phase exfoliation (LPE) methods.[124,127–129] The exfoliation of GeSe crystal has been experimentally established for both fundamental and applied research.[68,101–104,107–109,130,131] In comparison to its phosphorene analogues, the "black-phase" 2D GeSe structure shows a superior oxidation resistance,[68,132,133] with activation energies for the chemisorption of O_2 on its surface of 1.44 eV (more than twice of the value calculated for phosphorene).[133] Moreover, theoretical studies reported that the presence of H_2O molecules does not influence the oxidation process of Ge-based monochalcogenides,[133] which is different from the cases of isostructural phosphorene[133–135] and group-IIIA metal monochalcogenides (*e.g.*, InSe[136–138] and GeSe[139,140]). Therefore, these results advise a feasible use of 2D GeSe into photo(electro)chemical devices. To this purpose, the optoelectronic properties of the exfoliated GeSe can be tuned by varying the number of layers.[62,68] In fact, theoretical calculations demonstrated a *c*-axis confinement-induced optical bandgap (E_g) blue-shift,[62,68] showing an indirect bandgap in the bulk (between 1.1 and 1.2 eV)[141–143] and a direct bandgap in the monolayer (> 1.9 eV).[62,68] This E_g evolution from bulk to monolayer resembles the one exhibited by several group-VI transition metal dichalcogenides[144] (*e.g.*, MoS_2,[145–147] and $MoSe_2$[148]). Additionally, the E_g of single-/few-layer GeSe flakes is larger than the minimum energy required for the water splitting reaction (*i.e.*, 1.23 eV).[23] Even more, the number of layers in 2D GeSe determines the energy of conduction band minimum (CBM) and valence band maximum (VBM), which can be adjusted to fulfil the fundamental requirements for a water splitting photo(electro)catalysts, *i.e.*: 1) CBM energy (E_{CBM})> reduction potential of H^+/H_2 ($E(H^+/H_2)$), 2) VBM energy (E_{VBM}) < reduction potential of O_2/H_2O ($E(O_2/H_2O)$).[61,62,68] The interest for 2D GeSe as a photo(electro)catalyst also arises from its unusually strong visible-light absorbance (absorption coefficient up to 10^5 cm^{-1} in the visible spectral range).[149] The latter have been ascribed to the multiple electronic bands that are displayed near both VBM and CBM.[62,149] These electronic bands originate large joint density of states, which gives rise to a large probability of optical transitions across the energy gap.[97,143] Moreover, the electronic structure of GeSe results in low excitonic binding energy, predicted to be even lower than 100 meV,[62,97] and indicating efficient excitons dissociation in free charges.[62,97] Even more, the GeSe charge carries have high charge carriers mobility (theoretical values between 10^2 and 10^4 cm^2 V^{-1} s^{-1} for electrons,[62,150–152] between 1 and 10^3 cm^2 V^{-1} s^{-1} for holes[62,104,150,151,153]), facilitating their migration to the material surface, in which the redox processes take place.[62]

Stimulated by the predicted properties of 2D GeSe, we report the first experimental demonstration of the photo(electro)catalytic activity of single-/few-layer GeSe flakes in different aqueous media, ranging from acidic to alkaline solutions (*i.e.*: 0.5 M H_2SO_4, pH 0.3; 1 M KCl, pH 6.5; 1 M KOH, pH 14). Theoretical calculations were used to evaluate the electronic structures of single- and few-layer GeSe flakes and bulk GeSe. We describe the PEC working mechanisms of the photoelectrode based on GeSe nanoflakes with heterogeneous morphological properties such as lateral size and thickness, resulting in different (opto)electronic and photocatalytic properties. We reveal that GeSe nanoflakes with different thicknesses in nanoporous electrodes can act as different light absorbers in nanoscale tandem systems, mimicking photosynthetic systems (similarly to bio-inspired molecular photocatalysts)[154,155], by creating monolithic "all-solid-state Z-scheme water splitting pathways".[156–159] These expectations are experimentally proved on photoelectrodes fabricated through the spray-coating of single- and few-layer GeSe flakes, which are produced through LPE of synthetized "black-phase" GeSe crystal in environmentally friendly solvent (*i.e.*, isopropyl alcohol –IPA–). The electrochemical characterization of our GeSe-based photoelectrodes proves

both photoanodic and photocathodic responses in aqueous media, allowing PEC-type photodetectors for visible light to be conceived. Next, GeSe photoelectrodes are characterized after simulated sunlight for water splitting reactions, hydrogen evolution reaction (HER) and oxygen evolution reaction (OER).

RESULTS AND DISCUSSION

Understanding of structural, optoelectronic, and catalytic properties of the GeSe nanoflakes. The thermodynamic requirements for a water splitting photocatalyst are $E_{VBM} < E(O_2/H_2O)$ and $E_{CBM} > E(H^+/H_2)$ for OER and HER, respectively.[23,160] Therefore, the electronic structure calculation by means of DFT with generalized gradient approximation (GGA-PBE96)[161] and Heyd-Scuseria-Ernzerhof hybrid exchange-correlation functional (HSE06)[162] for bulk GeSe (B-GeSe) and single-/few-layer GeSe (xL-GeSe, x = 1; 2; 4 and 6) (see details in the Experimental Section, Supporting Information) were carried out to verify that GeSe nanoflakes fulfil energetic requirement for PEC water splitting. A clear feature of the ground state polymorph of B-GeSe (space group *Pnma*) is that it is not only isostructural but also isoelectronic with black phosphorus.[68,71] Therefore, as shown in Figure 1a, B-GeSe reveals noticeable similarities to the parent structure of black phosphorus.[68] Nevertheless, compared to black phosphorous, the difference in electronegativities and hence in on-site energies of Ge- and Se-4*s* and 4*p* valence orbitals imposes a larger and indirect bandgap (1.35 eV), as well as a larger energy separation between the Se-4*s* band (centered at 14 eV below the Fermi level $-E_F-$) and the topmost valence band of predominant Se 4*p* character (spreading from E_F down to –6 eV).[97,143] Near to the bottom of this valence band there is a Ge-4*s* band arising from Ge(2+)-4s^2 electron configuration. The comparison of the band dispersion for B-GeSe (Figure 1a) and 1L-GeSe (Figure 1b) shows a bandgap broadening with decreasing the number of layers (from 1.35 eV in B-GeSe to 1.80 eV in 1L-GeSe). In both cases, the band width of ~3 eV and its hybridization with Se-4*p* states indicate that Ge-4s^2 pair is far from being non-bonding and is less stereoactive than P-3s^2 in black phosphorous or phosphorene.[163,164]

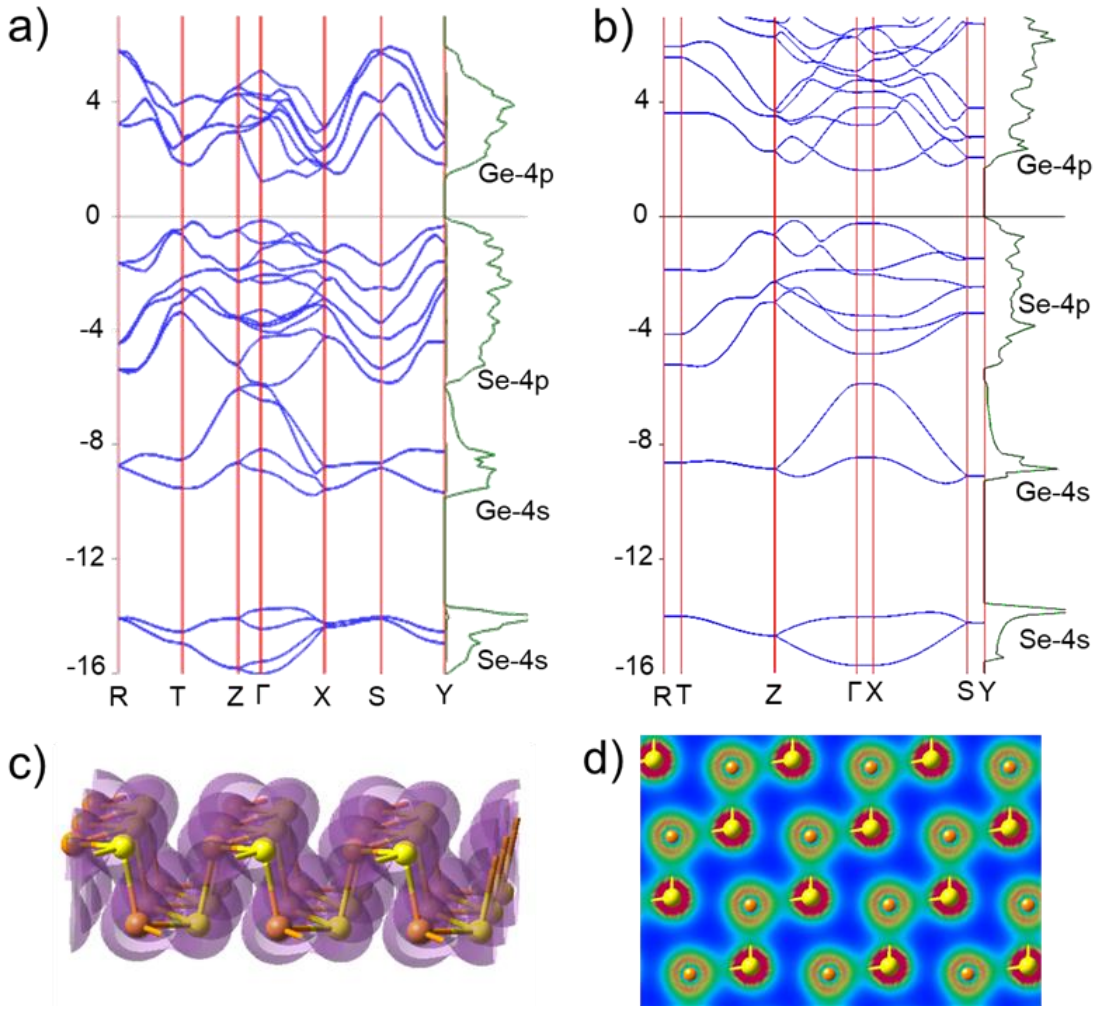

Figure 1. a,b) Band dispersion along principal directions of the first Brillouin zone and density of states for B-GeSe and 1L-GeSe, respectively. c) 3D isosurface of the electron density = –0.3 *e* Å^{-3}. d) Electron density distribution in 2D cross section over one Ge-Se layer.

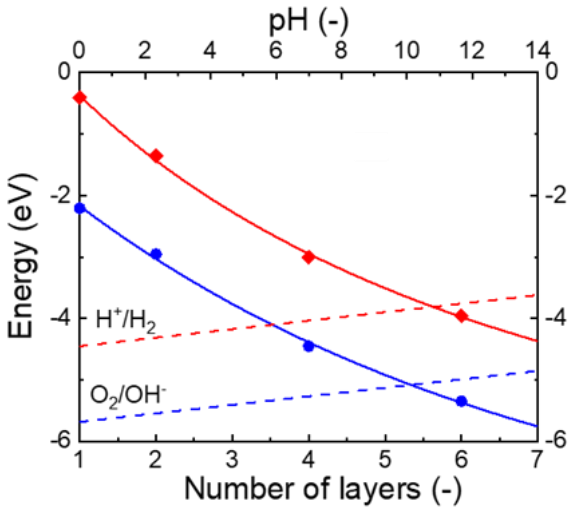

Figure 2. E_{VBM} (lower solid curve — and ● symbols) and E_{CBM} (upper solid curve — and ♦ symbols) of GeSe as a function of its layer number, compared with the potentials of water splitting ($E(H^+/H_2)$ and $E(O_2/H_2O)$) as a function of pH.

These attributes are further supported by the plots of electron density (Figure 1c and Figure 1d), revealing a nearly spherical distribution around Ge atoms (the red spots in panel d correspond to semi-core Ge-3*d* states). By contrast, the Ge-4*p* orbitals are unoccupied and they give rise to three different anisotropic conduction bands per Ge atom in the unit cell. The resulting spatial separation of the photogenerated carriers (*i.e.*, holes on Se and electrons on Ge) could be effective to suppress the electron-hole recombination in GeSe, promoting efficient photo(electro)catalytic responses.[165] The work function (WF) evolution of xL-GeSe with the number of layers was also elucidated through DFT calculations, showing WF values from 2.2 eV for 1L-GeSe to 5.3 eV for 6L-GeSe, and the upper limit value of 6.5 eV for B-GeSe. The values of bandgap were combined with the calculated WFs to construct the plot of E_{VBM} and E_{CBM} *vs.* the vacuum level, aiming to evaluate E_{VBM} and E_{CBM} of xL-GeSe and B-GeSe relatively to $E(O_2/H_2O)$ and $E(H^+/H_2)$, respectively.

Figure 2 reports E_{CBM} and the E_{VBM} of xL-GeSe as functions of the number of layers, while showing the $E(H^+/H_2)$ and $E(O_2/H_2O)$ as functions of the pH. The theoretical pH window satisfying the condition $E_{CBM} > E(H^+/H_2)$ and $E_{VBM} < E(O_2/H_2O)$ for HER and OER, respectively, corresponds to the pH range ~10.2–10.8 and the number of layers ~5–6. However, xL-GeSe with x < 6 fulfil the HER photocatalyst requirement independently of the pH. *Vice versa*, xL-GeSe with x ≥ 6 can satisfy the HER photocatalyst requirement. Therefore, GeSe nanoflakes with different thickness can be interfaced to act as nanoscale tandem systems, in which the thinner nanoflakes (*e.g.*, x-GeSe with x ≤ 4) preferably operate as HER-photocatalysts, while the thicker ones (*e.g.*, x-GeSe with x >4) can catalyze the OER (depending on the pH of the medium). By creating monolithic "all-solid-state Z-scheme water splitting pathways",[156–159] such GeSe systems could mimic the working processes of photosynthetic structures.[154,155] The van der Waals (vdW) interactions represent an essential feature in the modelling of GeSe, since they held together the different layers in the bulk stacks.[166,167] Our DFT calculations using GGA-PBE96 and including the vdW dispersion correction through the DFT-D3 method reveal more negative energy (by 25.5 kJ mol^{-1}) of B-GeSe compared to 1L-GeSe. Moreover, the surface energies obtained from the slab structures calculations decrease from 250 mJ m^{-2} for 1L-GeSe to 226 mJ m^{-2} for 6L-GeSe. By polynomial fitting of the data, the surface energy can be estimated to be ~220 mJ m^{-2} for the B-GeSe (001) surface. This value comparable to other p-block chalcogenides, such as GaSe (145 mJ m^{-2}),[58] and graphene (185 mJ m^{-2}).[120] Being the cleavage energy twice the surface energy, our theoretical data support that xL-GeSe can be produced by cleaving the B-GeSe, similarly to the exfoliation of other type of layered materials.[120]

Synthesis of exfoliation GeSe crystals and material characterization. Orthorhombic (*Pnma*) GeSe crystals were produced through direct synthesis followed by slow cooling of melt granules of Ge and Se elements.[168] Briefly, powders of Ge and Se with an elemental stoichiometry of 1:1 were inserted in a quartz glass ampoule, afterward evacuated, sealed and heated at 800 °C (*i.e.*, above melting temperature of GeSe) for 1 h (heating rate = 5 °C min^{-1}). The obtained products were cooled down to room temperature (cooling rate = 0.3 °C min^{-1}), obtaining the GeSe crystals. Figure 3a shows a photograph of a representative GeSe crystal, together with its crystal structure consisting of double-layer slabs of Ge-Se in a zig-zag configuration, separated from one another by a van der Waals gap.[91,169] The morphology of the GeSe crystals was evaluated by scanning electron microscopy (SEM) coupled with energy-dispersive X-ray spectroscopy (EDS). The high-magnification SEM image of an edge of a fragment of GeSe crystal (Figure 3b) evidences its layered structure. The SEM/EDS analysis (Figure 3c and Table S1) shows a slight excess of Ge (Ge-enriched phases) of the GeSe crystals (Ge-to-Se atomic ratio ~1.2). The stoichiometric excess of Ge is associated to the presence of corresponding oxides (*i.e.*, GeO_2 and GeO), which could form from the oxidation of Ge reactant residuals after air exposure.[170,171]

The GeSe nanoflakes were obtained through the LPE of pulverized GeSe crystals in anhydrous IPA. Importantly, IPA has been previously used to successfully exfoliate other Ge-based monochalcogenides (*i.e.*, GeS)[172] or group-IIIA metal monochalcogenides (*e.g.*, GaSe[58], GaS[173] and InSe[174,175]). Moreover, it circumvents the processability issues related to the use of high-boiling point and toxic solvents often used for the exfoliation of layered materials,[176,177] *e.g.*, *N*-Methyl-2-Pyrrolidone (NMP) for graphene[178,179] and several metal chalcogenides[180–182]. Subsequently, the dispersion was centrifuged in order to separate the un-exfoliated pieces of crystals (sediment) from the GeSe nanoflakes (process known as sedimentation-based separation –SBS–),[183–185] which were collected by extracting 80% of the supernatant. Transmission electron microscopy (TEM) and atomic force microscopy (AFM) analyses were performed to investigate the morphology of the GeSe nanoflakes. Figure 3d shows a TEM images of the GeSe nanoflakes, which display irregular shapes with sharp edges. The statistical analysis of their lateral sizes (Figure 3e) shows values ranging from 15 to 180 nm and following a log-normal distribution peaked at ~36 nm.

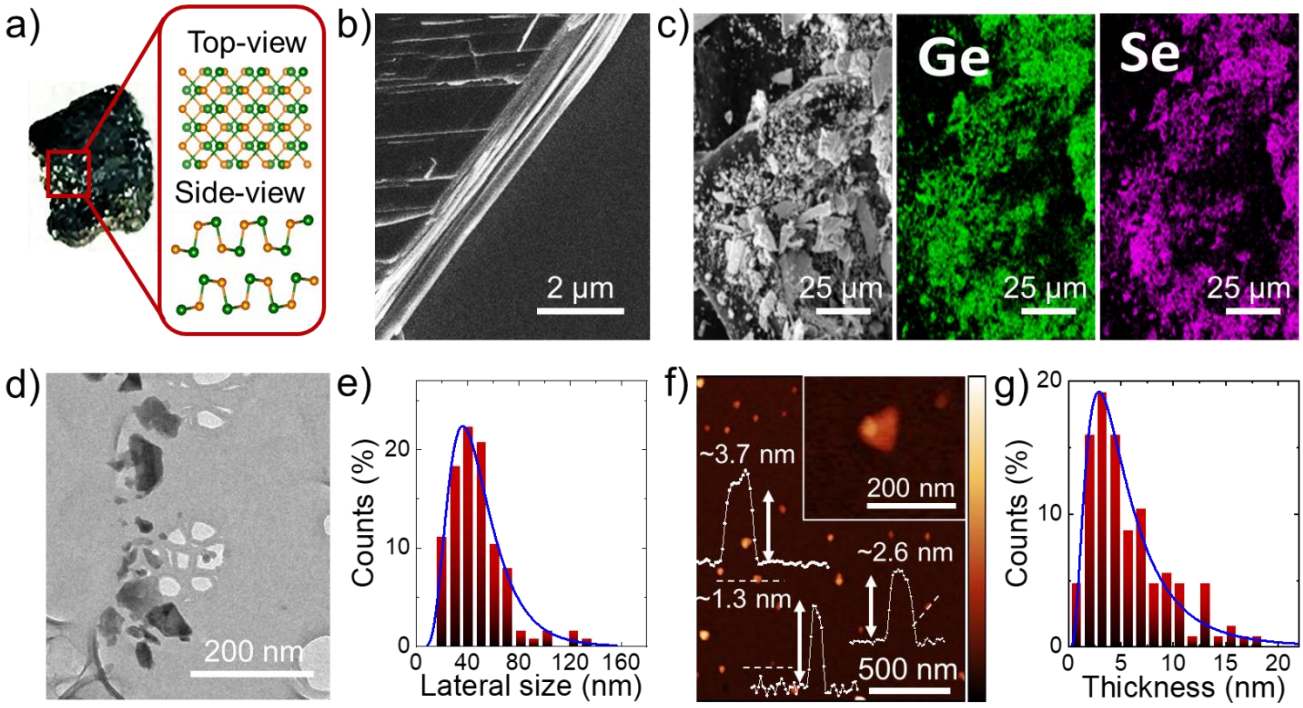

Figure 3. a) Photograph of a GeSe crystal synthesized through controlled cooling method. The orthorhombic (*Pnma*) structure of the GeSe crystal is also shown. b) SEM image of a fragment of GeSe crystal, evidencing its layered structure. c) SEM image of fragments of GeSe crystals and the corresponding EDS maps for Ge (K_α = 9.9 eV, green) and Se (L_α = 1.4 eV, violet). d) TEM image of the GeSe nanoflakes produced through LPE of pulverized GeSe crystal. e) TEM statistical analysis of the lateral dimension of representative GeSe nanoflakes. f) AFM image of representative GeSe nanoflakes. Height scale bar: 10 nm. The height profiles of two sections are also shown, exhibiting the presence of single-/few-layer flakes. g) AFM statistical analysis of the thickness of the GeSe nanoflakes.

Figure 3f reports an AFM image of various nanoflakes, with their height profiles (values between 1.1. and 7.5 nm). The statistical analysis of the thicknesses of the nanoflakes (Figure 3g) indicates that the values follow a log-normal distribution peaked at 2.8 nm. By considering an (experimental) AFM thickness of monolayer GeSe between 1 nm and 1.5 nm,[186] close to calculated values,[91,187] our AFM data indicates that the exfoliated sample is predominantly made of few (≤ 5)-layer flakes. However, either single layer or multi (> 5)-layer flakes are present, giving a mixture of nanoflakes with different optoelectronic properties (as predicted by the DFT calculations discussed above). X-ray diffraction (XRD) patterns of GeSe bulk and nanoflakes (Figure 4a) confirm the orthorhombic (*Pnma*) structure of bulk GeSe with the following lattice parameters: a = 10.8200 Å, b = 3.8520 Å, c = 4.4030 Å (ICDD card Nr. 33-582). Since no extra peaks attributed to oxides appear in the XRD pattern of exfoliated samples, we conclude that the LPE in anhydrous IPA effectively preserve the native structural properties of the GeSe bulk counterpart. The *Pnma* structure of the exfoliated sample was also assessed by selected-area electron diffraction (SAED) analysis of the TEM image of GeSe nanoflakes (Figure S1). The structural properties of the GeSe bulk and nanoflakes were further evaluated through Raman spectroscopy. The group theory predicts 12 Raman active optical modes for the D_{2h}^{16} space group of orthorhombic (*Pnma*) GeSe, *i.e.*: $4A_g + 2B_{1g} + 4B_{2g} + 2B_{3g}$.[188–190] Figure 4b shows the Raman spectra (excitation wavelength –λ_{exc}– = 633 nm) of the bulk and the exfoliated Ge samples, focusing on the spectral range of the most intense Raman peaks at ~152 cm^{-1}, ~176 cm^{-1} and ~190 cm^{-1}. These peaks are respectively attributed to the out-of-plane vibration mode B_{3g}^1 and two in-plane vibration modes A_g^2 and A_g^1,[188–190] as reported in previous studies using the same λ_{exc}[191,192] (A_g^2 is often not discussed in literature since it is almost negligible for λ_{exc} = 532 nm[190,191]). The comparison of our Raman spectra indicates that the ratio between the intensity of B_{3g}^1 and A_g^1 decreases with decreasing the thickness of the GeSe nanoflakes, in agreement with previous studies.[68,186] In addition, A_g^2 is slightly blue-shifted with decreasing the thickness of the GeSe crystals, while B_{3g}^1 and A_g^1 approximately retain their peak positions (see quantitative Raman analysis in Figure S2). Although isostructural analogues of GeSe (*e.g.*, black phosphorous) can exhibit reproducible thickness-dependent shifts of their Raman peaks as a consequence of the variation of the inter-layer forces when the number of layer changes,[193,194] discordant results have been reported for GeSe.[68,186] Therefore, contrarily to graphene and many 2D crystals and hybrid nanostructures,[195–197] caution is still needed when Raman spectroscopy is used as a tool for the precise determination of the thickness of exfoliated GeSe. More importantly for our purposes, GeSe nanoflakes do not exhibit any peaks attributed to Raman active modes of other species beyond GeSe (*e.g.*, GeO_2 or crystalline Se modes at ~420 cm^{-1} [198,199] and ~240 cm^{-1},[200] respectively), further supporting that the LPE in IPA does not cause any relevant oxidation effects, in agreement with XRD (Figure 4a) and X-ray photoelectron spectroscopy (XPS) analysis (Figures S3 and Figure S4, respectively). The E_g of the GeSe nanoflakes was assessed through diffusive reflectance spectroscopy (DRS) using the Kubelka-Munk theory of the diffusive reflectance *(R)*.[201,202]

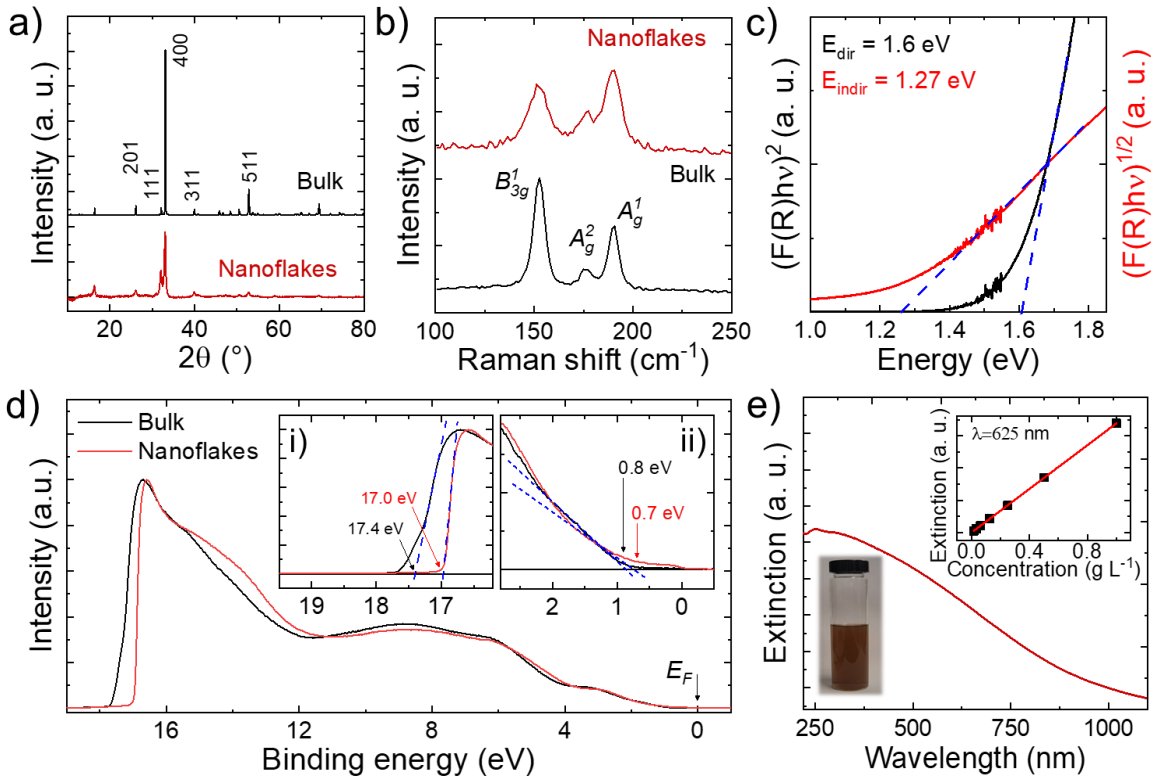

Figure 4. a) XRD and b) Raman spectra (excitation wavelength = 633 nm) of GeSe bulk (fragments of the as-synthetized GeSe crystal) and nanoflakes. The panels respectively report the diffraction peaks and the Raman modes attributed to the orthorhombic structure of the GeSe. c) $(F(R)hv)^n$ *vs.* hv (Tauc plots) for the GeSe nanoflakes for both direct (n = 2) and indirect inter-band transitions (n = 0.5). d) UPS spectra for GeSe bulk (fragments of the as-synthetized GeSe crystal) and nanoflakes (the binding energy is relative to the E_F, *i.e.*, E_F = 0 eV). The inset panel i) shows the enlargement of the secondary electron cut-off region of the spectra, while the inset panel ii) reports the region near the E_F (*i.e.*, VBM region) of the spectra. e) Optical extinction spectrum $Ext(\lambda)$ of the LPE-produced GeSe nanoflake dispersion, whose photograph is also shown in the panel. The top-right inset panel reports the Ext(625 nm) *vs.* c plot.

In particular, the E_g can be estimated by fitting the linear part of $(F(R)hv)^n$ *vs.* hv (Tauc Plot) with $(F(R)hv)^n = Y(hv - E_g)$ (Tauc relation), in which $F(R)$ is the Kubelka –Munk function, defined as $F(R) = (1-R)^2/2R$, h is Planck's constant, v is the photon's frequency, and Y is a proportionality constant.[201,202] The value of n specifies the type of the electronic transitions, distinguishing between direct (n = 2) and indirect inter-band transitions (n = 0.5).[203–205] Figure S5 reports the R spectrum of a film of GeSe nanoflakes deposited on quartz substrate. Figure 4c show the corresponding Tauc plots for both n = 2 and n = 0.5, from which we estimated a direct E_g of 1.27 eV and an indirect E_g of 1.60 eV, respectively. These E_g values agree with those calculated through DFT simulations and resemble those previously reported for few-layer GeSe flakes.[68,186] Noteworthy, our films are made of GeSe with polydisperse morphology characteristics, which means that the optical features of the thickest nanoflakes could experimentally screen those of thinnest nanoflakes, which shows the highest E_g.[58,206] The WF, and the E_{VBM} of the GeSe bulk and nanoflakes were determined through ultraviolet photoelectron spectroscopy (UPS).[203] Figure 4d reports the He I (21.22 eV) UPS spectra measured for the GeSe bulk and nanoflakes. The secondary electron cut-off region of the spectra (inset panel i) show that the cut-off energies are ~17.4 eV for GeSe bulk and ~17.0 eV for GeSe nanoflakes, corresponding to a WF of 3.8 eV for GeSe bulk and 4.2 eV for GeSe nanoflakes. The region near the E_F (*i.e.*, VBM region) of the UPS spectra (inset panel ii) reveals that E_{VBM} is -4.6 eV for GeSe bulk and -5.0 eV for GeSe nanoflakes. Contrary to our DFT calculations, these results indicated that the VBM of the nanoflakes is deeper than the one of bulk. Noteworthy, the WF and the band gap values for surface states can be substantially affected by chemical modification of the surface due to interaction with the surroundings, thus explaining discrepancies between experimental and theoretical data. The measured E_{CBM} of the GeSe nanoflakes, calculated by assuming the E_g previously estimated by the Tauc analysis, is 3.7 eV, which resembles the values theoretically derived for 5L GeSe flakes. As commented above for the Tauc analysis, the electronic characteristics attributed to the thinnest nanoflakes (*i.e.*, single-/bi-layer flakes) could be experimentally inaccessible through UPS measurements of a sample with nanoflakes having different thickness,[58,206,207] being the thicker (and larger) nanoflakes the main contributors to weight (or atomic) composition. The concentration of the as-produced GeSe flakes dispersion was first measured by weighting the solid material content in a known volume of the dispersion, giving a value of 0.22 ± 0.02 g L^{-1}. The extinction coefficient of the GeSe nanoflakes was estimated using the Lambert-Beer law: $Ext(\lambda) = \varepsilon(\lambda)cl$, in which λ is a given optical wavelength, $Ext(\lambda)$ is the optical extinction at the given λ, $\varepsilon(\lambda)$ is the extinction coefficient at the given λ, c is the material concentration and l is the optical path length.[208] In fact, by measuring the optical extinction spectra of controlled dilutions/concentrations of the as-produced GeSe nanoflake dispersion, $\varepsilon(\lambda)$ is calculated from the slope of $Ext(\lambda)$ *vs.* c plot, being: slope = $\varepsilon(\lambda)l$. Once known $\varepsilon(\lambda)$, c can be also precisely controlled among different batches of materials, being $c = Ext(\lambda)/(\varepsilon(\lambda)l)$.

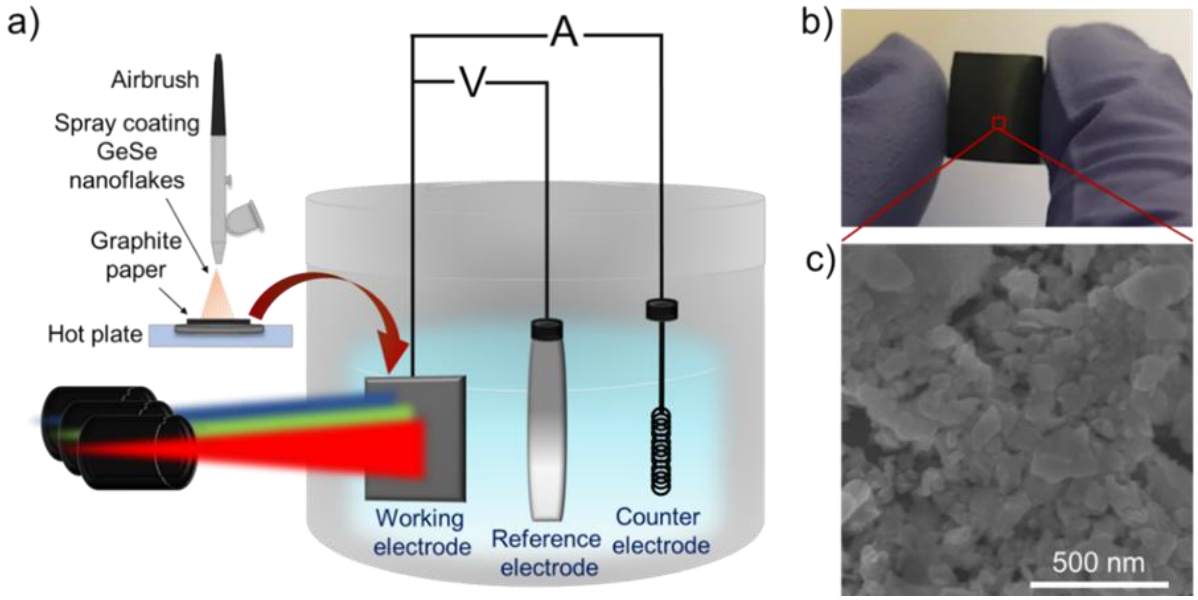

Figure 5. a) Schematic diagram of the experimental setup for electrochemical characterization of the GeSe photoelectrodes, which were produced by spray coating the GeSe nanoflakes onto a graphite paper substrate, acting as the current collector. b) Photograph of a GeSe photoelectrode, which was manually bent to its mechanical flexibility, and c) its corresponding top-view SEM image.

Figure 4e shows the optical extinction spectrum of the as-produced GeSe nanoflakes, which are capable to absorb the solar radiation in broad spectral range (UV-visible and near-infrared (<1100 nm) wavelengths). The inset panel reports the *Ext*(625 nm) vs. c plot, whose linear fitting provides a slope corresponding to a ε(625 nm) of 136.0 L g^{-1} m^{-1}.

Photoelectrochemical properties of the GeSe nanoflakes and their PEC-type photodetectors. On the basis of our theoretical investigation of the photo(electro)catalytic properties of the single-/few-/multi-layer GeSe flakes, the PEC properties of the LPE-produced GeSe nanoflakes were investigated for water splitting reactions (HER and OER) in different aqueous media, ranging from acidic to alkaline solutions (*i.e.*: 0.5 M H_2SO_4, pH 0.3; 1 M KCl, pH 6.5; 1 M KOH, pH 14). The electrodes were produced by spray coating the GeSe nanoflake dispersion on graphite paper (mass loading of GeSe nanoflakes = 0.1 mg cm^{-2}) and tested in a three-electrode configuration system (Figure 5a). To the best of our knowledge, a precise evaluation of the PEC properties of exfoliated GeSe materials in aqueous media is still missing, and only ref. [68] has reported a preliminary PEC characterization of few-layer GeSe flakes in 0.1 M Na_2SO_4. Figure 5b reports a photograph of a sprayed GeSe photoelectrode, which was bent to evidence its mechanical flexibility. Figure 5c reports a top-view SEM image of a GeSe photoelectrode, showing a film made of nanoflakes preferentially placed with a horizontal position of their planes with respect to the substrate plane. The GeSe photoelectrodes were first evaluated as PEC-type photodetectors for three different illumination wavelengths in the visible spectral range, namely 455, 505 and 625 nm. These illumination wavelengths correspond to energies above the E_g of our GeSe nanoflakes, *i.e.*, 1.27 eV (Figure 4c). Noteworthy, a photoresponse for these wavelengths can be used for the realization of colorimeters, *i.e.*, three-channeled device that quantify the tristimulus red, green, and blue components by means photodetectors with spectral responsivity resembling the International Commission on Illumination (CIE)'s color matching functions (*i.e.*, the numerical description of the chromatic responses of the CIE 1931 Standard Observer observer).[209–211] Figure 6a shows the responsivity vs. potential plots derived from linear sweep voltammetry (LSV) measurements for GeSe photodetectors for illumination wavelengths (intensity = 63.5 µW cm^{-2}) in 0.5 M H_2SO_4, 1 M KCl and 1 M KOH. In order to avoid the photoelectrode degradation, the applied potentials were limited within a region corresponding to absolute dark current density inferior to 50 µA cm^{-2} for both cathodic and anodic operations (except for the anodic scans in 1 M KOH, in which higher dark current density were considered to display responsivities higher than 1 mA W^{-1}). In all the investigated media, the responsivity of the photodetectors increases with decreasing the illumination wavelength. This behavior indicates that the photons with the highest energy (*e.g.*, ~2.7 eV for illumination wavelength = 455 nm) can efficiently excite the GeSe nanoflakes (in agreement with the DRS analysis, Figure 4c), including the thinnest ones, which exhibit the highest bandgap (1.80 eV for single-layer flakes, Figure 1b). For cathodic operation in 0.5 M H_2SO_4, the GeSe photodetectors reach a responsivity of 316.6 and 95.5 mA W^{-1} at -0.5 and +0.8 V *vs.* RHE, respectively. In 1 M KCl, the photoelectrodes reach remarkable responsivity of 234.5 and 248.3 mA W^{-1} at -0.1 and +0.9 V *vs.* RHE, respectively. The responsivity values of our GeSe photodetectors in both 0.5 M H_2SO_4 and 1 M KCl approach those of self-powered commercial UV–Vis photodetectors, including GaP or Si photodiodes.[212] In addition, the responsivity is higher than the ones achieved by self-powered and low-voltage solution-processed photodetectors (see Table S2 in the Supporting Information), including recent PEC-type photodetectors using group-IIIA metal monochalcogenides (*e.g.*, InSe[60] and GaSe[58]).

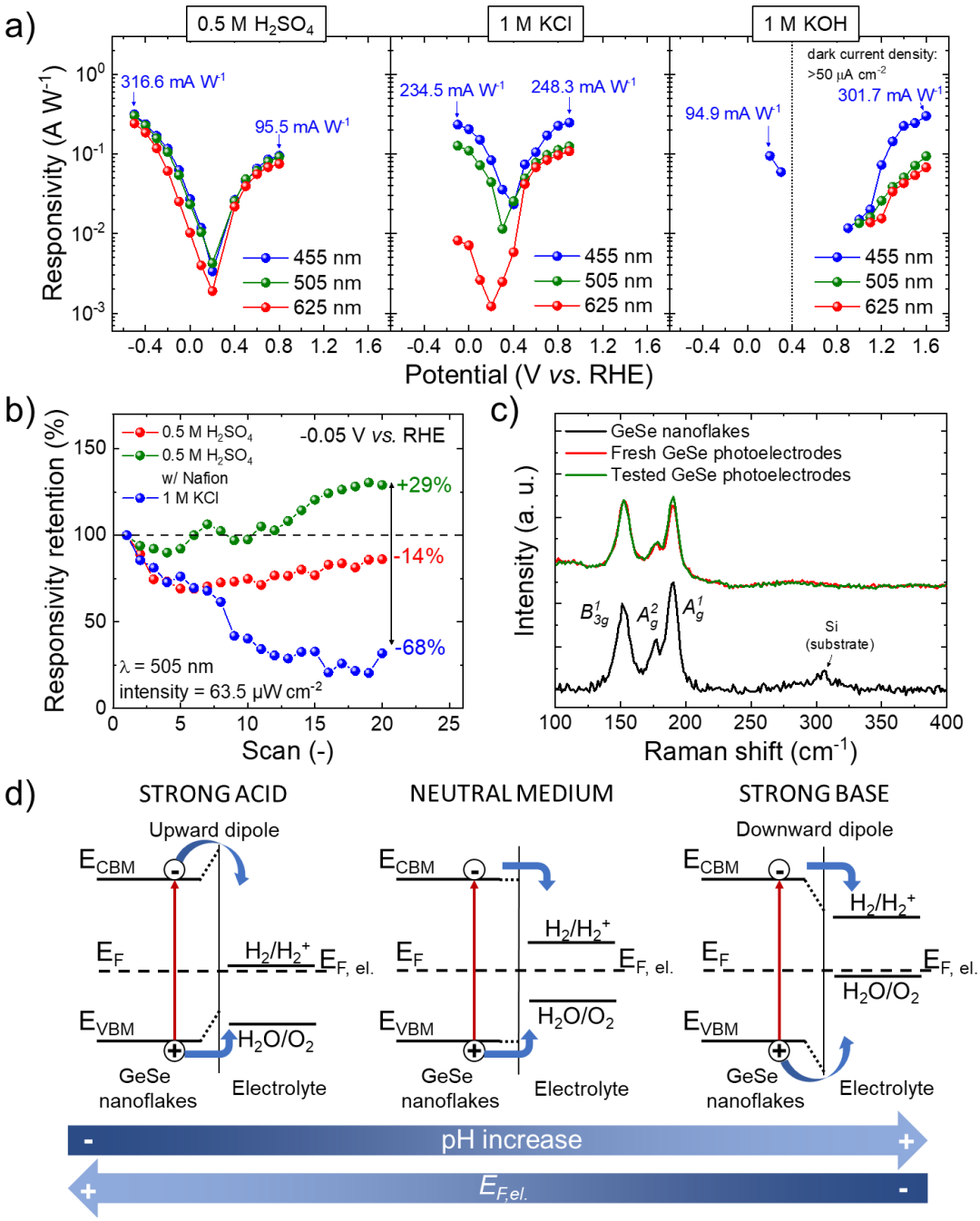

Figure 6. a) Responsivity of PEC-type GeSe photodetectors as a function of the applied potential in the investigated media (*e.g.*, 0.5 M H_2SO_4, 1 M KCl, 1 M KOH) upon three different illumination wavelengths in the visible spectral range: 455 nm, blue; 505 nm, green; 625 nm, red. Light intensity: 63.5 µW cm^{-2}. b) Responsivity retention of the GeSe photodetectors in 0.5 M H_2SO_4 and 1 M KCl during cathodic operation (applied potential = -0.05 V *vs.* RHE). c) Raman spectra (λ_{exc} = 633 nm) of the GeSe nanoflakes deposited on Si substrate, fresh GeSe photoelectrodes, and tested Ge photoelectrodes (*i.e.*, photoelectrodes measured after 20 cathodic LSV scans, as shown in panel b). d) Sketch of the energy diagram at the GeSe nanoflake/electrolyte interfaces, pointing out the formation of upward and downward dipoles in strong acids and bases, respectively.

Noteworthy, the highest recorded responsivity (*i.e.*, 316.6 mA W^{-1}) corresponds to an external quantum efficiency (EQE) (calculated as EQE = 100×(responsivity/λ)×1240 W nm A^{-1}, in which λ is given in nm and the responsivity in A W^{-1}) of 86.3%, thus approaching the theoretical performance limit for PEC-type photodetectors (*i.e.*, 100%).[213] The photoelectrodes in 1 M KOH display a cathodic responsivity of 94.9 mA W^{-1} at +0.2 V *vs.* RHE. Notably, the graphite paper (substrates) shows significant (dark) current densities (in the order of tens of µA cm^{-2}) during cathodic operation for potential inferior to +0.7 V *vs.* RHE (Figure S6). These current densities restrict the analysis of the PEC properties of GeSe nanoflakes for potential superior to +0.1 V *vs.* RHE. Although the anodic responsivity of the GeSe photodetectors in KOH can reach values up to 301.7 mA W^{-1} at 1.6 V *vs.* RHE, the high dark current density (> 100 µA cm^{-2}) suggest a possible corrosion of the photodetector materials. Since the graphite paper does not show significant current densities during anodic operation (Figure S7), the electrochemical reactivity of the photoelectrode materials can be mainly attributed to the GeSe nanoflakes. To preliminary asses the stability of our photodetectors, their responsivity was evaluated over

subsequent scans. During cathodic operation at -0.05 V *vs.* RHE (Figure 6b), the photodetectors exhibited the most stable responsivity in 0.5 M H_2SO_4. In addition, a sulfonated tetrafluoroethylene-based fluoropolymer-copolymer (namely Nafion) film atop the photocatalytic GeSe film was evaluated to contrast a possible delamination of the GeSe nanoflakes as the redox reaction occurs.[214] Consequently, the Nafion-coated photoelectrode did not exhibit any loss of responsivity, but on the contrary, it increases by +29%, possibly due to the hydration of the Nafion coating during subsequent LVS scans.[214,215] The chemical and structural integrity of the GeSe nanoflakes after stability test for cathodic operation in 0.5 M H_2SO_4 was further evaluated by Raman spectroscopy measurements (Figure 6c). The GeSe photoelectrodes show a Raman spectrum resembling the one measured on the as-produced GeSe photoelectrode and the GeSe nanoflakes (deposited onto a Si substrate). These results indicate that GeSe nanoflakes retain their initial structural properties during cathodic operation. By increasing the pH, the photodetectors rapidly degrade, especially in 1 M KOH, in which they cease to respond to light after two LSV scans. Figure S8 shows the chronoamperometry measurements performed on the GeSe photodetectors under 455 nm illumination at the fixed cathodic potential of -0.05 V *vs.* RHE in the most stable electrolyte conditions, *i.e.*, 0.5 M H_2SO_4 and 1 M KCl. In agreement with the LSV data, the GeSe photoelectrode retained its initial photocurrent in 0.5 M H_2SO_4, while a significant photocurrent degradation (~-50%) was observed in 1 M KCl. The degradation of the photodetectors was also observed during anodic operation (Figure S9), although the highest responsivity retention was again observed in 0.5 M H_2SO_4. Although the theoretically predicted oxidation resistance of 2D GeSe,[68,132,133] we cannot exclude that defective states in our nanoflakes can act as reactive sites triggering the oxidation processes. Prospectively, the production of undefective GeSe nanoflakes through optimized synthesis protocols may increase the stability and the reproducibility of the PEC performance of the GeSe nanoflakes.

Overall, our measurements revealed that GeSe nanoflakes can be used as photocatalyst for water splitting reactions, but precautions are needed when selecting the electrolytic medium to avoid degradation effects. Our results suggest that acidic media and cathodic operation are adequate working conditions to stably exploit the photocatalytic properties of the GeSe nanoflakes. By deeply analyzing the potential dependence of the responsivity, we point out that the GeSe photodetectors shows the best PEC performance at potential relevant for water splitting application (*i.e.*, potential between 0 and +1.23 V *vs.* RHE) in 1 M KCl. Since $E(H^+/H_2)$ and $E(O_2/H_2O)$ increase with increasing the pH, acidic and alkaline condition are commonly expected to increase the water splitting activity for HER and OER, respectively. However, the band bending or the dipole formation occurring at semiconductor (photocatalyst)/electrolyte interface can also significantly affect the PEC performance of a photoelectrode. The latter effects depend on both the nature of the semiconductor (*n*- or *p*-type) and the pH of the aqueous media, as sketched by the energy diagrams of the GeSe nanoflake/electrolyte interface in Figure 6d. In particular, for strong acidic media (*i.e.*, high H^+ concentration) and insufficient p-doping of the photocatalysts, an upward band bending/dipole results in an energy barrier that the electrons have to overcome to carry out HER.[216,217] An equivalent consideration can be drawn for explaining the downward band bending/dipole in strong alkaline media, in which the OER-activity of the GeSe starts at higher overpotential in comparison to those observed in both quasi-neutral and acidic media. Since the UPS analysis revealed that our GeSe nanoflakes are slightly *n*-type materials, the aforementioned effects could explain the best photoresponse of the GeSe photoelectrodes at potentials between 0 and +1.23 V *vs.* RHE in 1 M KCl. To validate this explanation, light intensity dependence of the cathodic responsivity was evaluated in both 0.5 M H_2SO_4 at fixed potential of 0 V *vs.* RHE (Figure S10), under which conditions the photodetectors have shown a satisfactory stability. Typically, the relationship between the photocurrent density and the light intensity follows the power equation photocurrent density $\propto$ (light intensity)$^{\gamma}$,[218,219] in which γ is a factor determining the response of the photocurrent to light intensity. A unity value for γ indicates the absence of charge recombination and trapping processes, while non-unity γ suggests a complex process of charge generation, recombination, and trapping phenomena within the photoactive material.[218,219] In 0.5 M H_2SO_4, the power law fit gives a γ of 0.56, indicating significant charge recombination of the photogenerated charges as originated by the presence of an interfacial dipole. Differently, in 1 M KCl the power law fits to the experimental data with γ equal to 0.83 (Figure S11). This value indicates a satisfactory utilization of the photogenerated charges to carry out the redox reaction. As expected for 2D materials, this effect can be attributed to the intrinsic maximization of the electrochemically accessible surface area,[28,58,220] as well as to the nearly zero distance between the photogenerated charges and the catalytic surface area.[28,58,220]

Based on the above PEC characterization, GeSe photoelectrodes were evaluated as either photocathodes or photoanodes for HER and OER, respectively, under chopped simulated sunlight (*i.e.*, AM 1.5G standard spectra, irradiance = 1000 W m^{-2}). Figure 7a,b show the cathodic and anodic LSV scans measured for GeSe photoelectrodes in 0.5 M H_2SO_4 and 1 M KCl, respectively. Noteworthy, 0.5 M H_2SO_4 and 1 M KCl media resulted in the highest photoelectrode photoresponses at 0 V *vs.* RHE and +1.23 V *vs.* RHE, respectively. The following Figures of Merit are used to quantify the photoresponse of the electrodes for water splitting reactions (*i.e.*, HER and OER): the negative (cathodic) photocurrent density at 0 V *vs.* RHE ($J_{0V\ vs.\ RHE}$), the positive (anodic) photocurrent density at +1.23 V *vs.* RHE ($J_{1.23V\ vs.\ RHE}$) and the photocurrent onset potential (VOP) (defined as the equilibrium potential of the photoelectrodes under simulated sunlight). For the cathodic LSV scan in 0.5 M H_2SO_4, the GeSe photoelectrode shows: $J_{0V\ vs.\ RHE}$ = -10.9 μA cm^{-2} and V_{OP} = +0.30 V *vs.* RHE. For the anodic LSV scans in 1 M KOH, the photoelectrode shows: $J_{1.23V\ vs.\ RHE}$ = +31.0 μA cm^{-2} and V_{OP} = +0.48 V *vs.* RHE. These results prove that the GeSe nanoflakes are promising materials to be used in water photoelectrolysis cells. Although it is beyond of the scope of the current work, our GeSe photoelectrodes could be further engineered by: 1) adding charge selective layers to selectively control the interfacial charge transfer for a single photocarrier species (holes or electrons), making them either photocathodes or photoanodes; 2) incorporating co-catalyst onto their surface to further accelerate the water splitting reaction (*e.g.*, 2D transition metal dichalcogenides for HER[221,222,223,224] and layered double hydroxide[225,226] or functionalized graphene[227,228] for OER); 3) using porous substrates (*e.g.*, carbon nanotubes),[229] which mechanically stabilize photocatalytic materials on their surfaces; 4)

optimizing the thickness and the morphology of the sprayed GeSe film, thus increasing the overall absorption of the solar light.

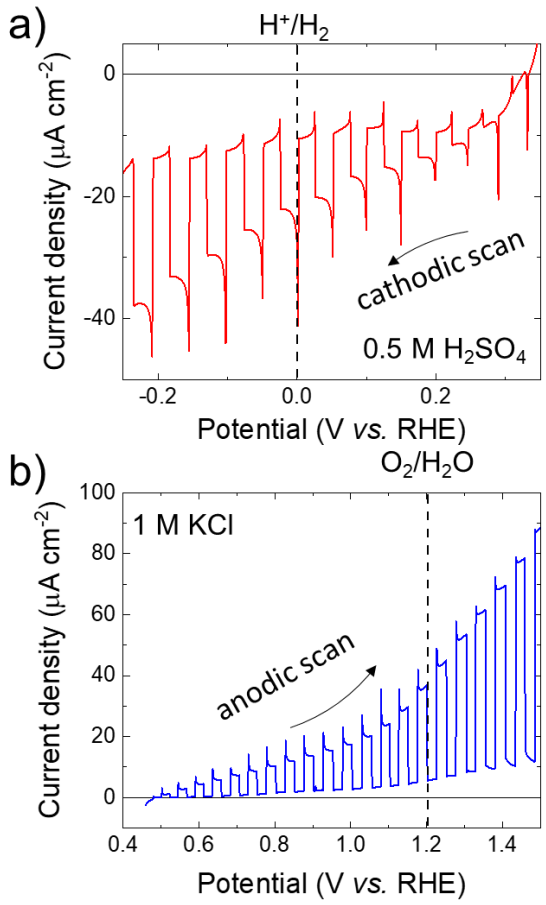

Figure 7. a,b) LSV curves measured for GeSe photoelectrodes for HER (cathodic scan) in 0.5 M H_2SO_4 and b) OER (anodic scan) in 1 M KCl, under chopped simulated sunlight (*i.e.*, AM 1.5G illumination). The redox potential for H^+/H_2 (0 V *vs.* RHE) and O_2/H_2O (+1.23 V *vs.* RHE) are also shown.

CONCLUSION

In summary, the electronic structure of GeSe has been theoretically studied using density functional theory (DFT) simulations. The calculated optical bandgap (E_g) values (1.80 eV for single-layer flake and 1.35 eV for multi-layer flakes) indicate that GeSe nanoflakes can optimally absorb the solar light. In addition, depending on the thickness and the pH, GeSe nanoflakes can fulfil one or both the water splitting requirements, *i.e.*, $E_{CBM} > E(H^+/H_2)$ and $E_{VBM} < E(O_2/H_2O)$. Our simulations show that GeSe nanoflakes with different thickness can be mixed in form of films to act as nanoscale tandem systems, in which the thinner nanoflakes operate as HER-photocatalysts, while the thicker ones perform the OER. Therefore, once coupled, GeSe nanoflakes in nanoporous films can intrinsically realize "all-solid-state Z-scheme water splitting pathways", mimicking complex photosynthetic systems. Based on this theoretical prediction, a mixture of GeSe nanoflakes with different thicknesses, including single-/few-/multi-layer flakes, has been produced through liquid-phase exfoliation (LPE) of a GeSe crystals in isopropyl alcohol (IPA). The GeSe photoelectrodes were produced by spray coating the as-produced GeSe nanoflake dispersion onto graphite papers, acting as the current collectors. The as-produced photoelectrodes were first investigated as photoelectrochemical (PEC)-type photodetectors in acidic (0.5 M H_2SO_4, pH 0.3), near neutral (1 M KCl, pH 6.5) and alkaline (1 M KOH, pH 14) media. In particular, the GeSe photodetectors reach responsivity up to 316.6 mA W^{-1} at -0.5 V *vs.* RHE, which corresponds to an external quantum efficiency of 86.3%. This value approaches the theoretical limit of 100% of PEC-type photodetectors. Importantly, the GeSe photocathodes also stably operate. By increasing the pH towards alkaline values, the GeSe photodetectors start to degrade during operation, especially under anodic potential conditions. Lastly, the GeSe photoelectrodes were evaluated as photocathodes and photoanodes for HER and OER under simulated sunlight. The GeSe photocathodes reach a photocurrent density at 0 V *vs.* RHE ($J_{0V\ vs.\ RHE}$) of -10.9 μA cm^{-2} in 0.5 M H_2SO_4, while GeSe photoanodes display a photocurrent density at +1.23 V *vs.* RHE ($J_{1.23\ V\ vs.\ RHE}$) of 31.0 μA cm^{-2} in in 1 M KCl. Overall, our evaluation of the photoelectrochemical (PEC) properties of GeSe nanoflakes in aqueous media can further spark the interest for novel type of water splitting photocatalysts based on group-IVA metal monochalcogenides. The engineering of GeSe photoelectrodes by optimizing the photocatalyst loading (*i.e.*, film thickness), as well as by incorporating charge selective layers or co-catalysts, could prospectively boost the PEC performance of GeSe nanoflakes achieved in this work. Nevertheless, the design of photoactive films composed by LPE-produced GeSe nanoflakes with different thicknesses, and thus different optoelectronic properties, could represent a straightforward approach to fabricate monolithic all-solid-state Z-scheme PEC devices.

ASSOCIATED CONTENT

Supporting Information

The Supporting Information is available free of charge on the ACS Publications website.

Experimental section and additional TEM/SAED, SEM-EDS, XPS, DRS, PEC characterizations (PDF)

AUTHOR INFORMATION

Corresponding Author

* E-mail: sebastiano.bellani@iit.it; francesco.bonaccorso@iit.it

Author Contributions

‡These authors contributed equally.

Funding Sources

This project has received funding from the European Union's Horizon 2020 research and innovation program under grant agreement No.785219-GrapheneCore2, the MSCA-ITN ULTIMATE project under grant agreement No. 813036 and the Bilateral project GINSENG between NSFC (China) and MAECI (Italy) (2018 - 2020), by Natural Science Foundation of Shandong Province (ZR2019QEM009). This work was supported by the Czech Science Foundation (GACR No. 20-16124J). Computational resources were supplied by the project "e-Infrastruktura CZ" (e-INFRA LM2018140) provided within the program Projects of Large Research, Development and Innovations Infrastructures. M.I.Z. received funding from PON

Research and Innovation 2014-2020 (CUP H25D18000230006) by Italian Ministry of University and Research.

ACKNOWLEDGMENT

We thank: the Materials Characterization Facility –Istituto Italiano di Tecnologia– for the support in XRD data acquisition/analysis; the Electron Microscopy facility –Istituto Italiano di Tecnologia– for the support in TEM data acquisition; the Clean Room facility –Istituto Italiano di Tecnologia– for the access to carry out SEM characterization. We also thank Stefano Bortolotti for taking care of cover art proposal.

ABBREVIATIONS

Photoelectrochemical (PEC), density functional theory (DFT), hydrogen evolution reaction (HER), oxygen evolution reaction (OER), conduction band minimum (CBM) and valence band maximum (VBM), isopropyl alcohol (IPA), liquid-phase exfoliation (LPE).

REFERENCES

(1) Kim, D.; Sakimoto, K. K.; Hong, D.; Yang, P. Artificial Photosynthesis for Sustainable Fuel and Chemical Production. *Angew. Chem. Int. Ed.* **2015**, *54* (11), 3259–3266.

(2) Lewis, N. S.; Nocera, D. G. Powering the Planet: Chemical Challenges in Solar Energy Utilization. *Proc. Natl. Acad. Sci.* **2006**, *103* (43), 15729–15735.

(3) Crabtree, G. W.; Lewis, N. S. Solar Energy Conversion. *Phys. Today* **2007**, *60* (3), 37–42. h

(4) Chu, S.; Fan, S.; Wang, Y.; Rossouw, D.; Wang, Y.; Botton, G. A.; Mi, Z. Tunable Syngas Production from CO2and H2O in an Aqueous Photoelectrochemical Cell. *Angew. Chem. Int. Ed.* **2016**, *55* (46), 14262–14266.

(5) Zhang, H.; Chen, G.; Bahnemann, D. W. Photoelectrocatalytic Materials for Environmental Applications. *J. Mater. Chem.* **2009**, *19* (29), 5089–5121.

(6) Meng, X.; Zhang, Z.; Li, X. Synergetic Photoelectrocatalytic Reactors for Environmental Remediation: A Review. *J. Photochem. Photobiol. C Photochem. Rev.* **2015**, *24*, 83–101.

(7) Daghrir, R.; Drogui, P.; Robert, D. Photoelectrocatalytic Technologies for Environmental Applications. *J. Photochem. Photobiol. A Chem.* **2012**, *238*, 41–52.

(8) Zhang, B.; Guo, L.-H. Highly Sensitive and Selective Photoelectrochemical DNA Sensor for the Detection of Hg2+ in Aqueous Solutions. *Biosens. Bioelectron.* **2012**, *37* (1), 112–115.

(9) Yue, Z.; Lisdat, F.; Parak, W. J.; Hickey, S. G.; Tu, L.; Sabir, N.; Dorfs, D.; Bigall, N. C. Quantum-Dot-Based Photoelectrochemical Sensors for Chemical and Biological Detection. *ACS Appl. Mater. Interfaces* **2013**, *5* (8), 2800–2814.

(10) Shu, J.; Tang, D. Current Advances in Quantum-Dots-Based Photoelectrochemical Immunoassays. *Chem Asian J.* **2017**, *12* (21), 2780–2789.

(11) Zang, Y.; Lei, J.; Ju, H. Principles and Applications of Photoelectrochemical Sensing Strategies Based on Biofunctionalized Nanostructures. *Biosens. Bioelectron.* **2017**, *96*, 8–16.

(12) Zhou, J.; Chen, L.; Wang, Y.; He, Y.; Pan, X.; Xie, E. An Overview on Emerging Photoelectrochemical Self-Powered Ultraviolet Photodetectors. *Nanoscale* **2016**, *8* (1), 50–73.

(13) Tian, W.; Wang, Y.; Chen, L.; Li, L. Self-Powered Nanoscale Photodetectors. *Small* **2017**, *13* (45), 1701848.

(14) Hosseini, S. E.; Wahid, M. A. Hydrogen Production from Renewable and Sustainable Energy Resources: Promising Green Energy Carrier for Clean Development. *Renew. Sustain. Energy Rev.* **2016**, *57*, 850–866.

(15) Dincer, I.; Acar, C. Review and Evaluation of Hydrogen Production Methods for Better Sustainability. *Int. J. Hydrogen Energy* **2014**, *40* (34), 11094–11111.

(16) Gregory, D. P. The Hydrogen Economy. *Sci. Am.* **1973**, *228* (1), 13–21.

(17) Crabtree, G. W.; Dresselhaus, M. S.; Buchanan, M. V. The Hydrogen Economy. *Phys. Today* **2004**, *57* (12), 39–44.

(18) Chen, K.; Wang, S.; He, C.; Zhu, H.; Zhao, H.; Guo, D.; Chen, Z.; Shen, J.; Li, P.; Liu, A.; Li, C.; Wu, F.; Tang, W. Photoelectrochemical Self-Powered Solar-Blind Photodetectors Based on Ga2O3 Nanorod Array/Electrolyte Solid/Liquid Heterojunctions with a Large Separation Interface of Photogenerated Carriers. *ACS Appl. Nano Mater.* **2019**, *2* (10), 6169–6177.

(19) Chen, D.; Wei, L.; Meng, L.; Wang, D.; Chen, Y.; Tian, Y.; Yan, S.; Mei, L.; Jiao, J. High-Performance Self-Powered UV Detector Based on SnO2-TiO2 Nanomace Arrays. *Nanoscale Res. Lett.* **2018**, *13*.

(20) Wang, B.; Huang, Z.; Tang, P.; Luo, S.; Liu, Y.; Li, J.; Qi, X. One-Pot Synthesized Bi 2 Te 3 /Graphene for a Self-Powered Photoelectrochemical-Type Photodetector. *Nanotechnology* **2020**, *31* (11), 115201.

(21) Liu, N.; Qiao, H.; Xu, K.; Xi, Y.; Ren, L.; Cheng, N.; Cui, D.; Qi, X.; Xu, X.; Hao, W.; Dou, S. X.; Du, Y. Hydrogen Terminated Germanene for a Robust Self-Powered Flexible Photoelectrochemical Photodetector. *Small* **2020**, *16* (23), 2000283.

(22) Li, J.; Wu, X.; Shirolkar, M. M.; Li, M.; Xu, C.; Wang, H. A High Performance ZnO Based Photoelectrochemical Cell Type UV Photodetector with [Co(Bpy)3]3+/2+ Electrolyte and PEDOT/ITO Counter Electrode. *RSC Adv.* **2017**, *7* (31), 18987–18992.

(23) Bellani, S.; Antognazza, M. R.; Bonaccorso, F. Carbon-Based Photocathode Materials for Solar Hydrogen Production. *Adv. Mater.* **2019**, *31* (9), 1801446.

(24) Zhu, S.; Wang, D. Photocatalysis: Basic Principles, Diverse Forms of Implementations and Emerging Scientific Opportunities. *Adv. Energy Mater.* **2017**, *7* (23), 1700841.

(25) Lianos, P. Review of Recent Trends in Photoelectrocatalytic Conversion of Solar Energy to Electricity and Hydrogen. *Appl. Catal. B Environ.* **2017**, *210*, 235–254.

(26) Faraji, M.; Yousefi, M.; Yousefzadeh, S.; Zirak, M.; Naseri, N.; Jeon, T. H.; Choi, W.; Moshfegh, A. Z. Two-Dimensional Materials in Semiconductor Photoelectrocatalytic Systems for Water Splitting. *Energy Environ. Sci.* **2019**, *12* (1), 59–95.

(27) Li, Y.; Li, Y.-L.; Sa, B.; Ahuja, R. Review of Two-Dimensional Materials for Photocatalytic Water Splitting from a Theoretical Perspective. *Catal. Sci. Technol.* **2017**, *7* (3), 545–559.

(28) Su, T.; Shao, Q.; Qin, Z.; Guo, Z.; Wu, Z. Role of Interfaces in Two-Dimensional Photocatalyst for Water Splitting. *ACS Catal.* **2018**, *8* (3), 2253–2276.

(29) Gan, X.; Lei, D.; Wong, K.-Y. Two-Dimensional Layered Nanomaterials for Visible-Light-Driven Photocatalytic Water Splitting. *Mater. Today Energy* **2018**, *10*, 352–367.

(30) Matsumoto, Y.; Koinuma, M.; Ida, S.; Hayami, S.; Taniguchi, T.; Hatakeyama, K.; Tateishi, H.; Watanabe, Y.; Amano, S. Photoreaction of Graphene Oxide Nanosheets in Water. *J. Phys. Chem. C* **2011**, *115* (39), 19280–19286.

(31) Yeh, T.-F.; Cihlář, J.; Chang, C.-Y.; Cheng, C.; Teng, H. Roles of Graphene Oxide in Photocatalytic Water Splitting. *Mater. Today* **2013**, *16* (3), 78–84.

(32) Xiang, Q.; Cheng, B.; Yu, J. Graphene-Based Photocatalysts for Solar-Fuel Generation. *Angew. Chem. Int. Ed.* **2015**, *54* (39), 11350–11366.

(33) Xie, G.; Zhang, K.; Guo, B.; Liu, Q.; Fang, L.; Gong, J. R. Graphene-Based Materials for Hydrogen Generation from Light-Driven Water Splitting. *Adv. Mater.* **2013**, *25* (28), 3820–3839.

(34) Naseri, A.; Samadi, M.; Pourjavadi, A.; Moshfegh, A. Z.; Ramakrishna, S. Graphitic Carbon Nitride (g-C 3 N 4)-Based Photocatalysts for Solar Hydrogen Generation: Recent Advances and Future Development Directions. *J. Mater. Chem. A* **2017**, *5* (45), 23406–23433.

(35) Jorge, A. B.; Martin, D. J.; Dhanoa, M. T. S.; Rahman, A. S.; Makwana, N.; Tang, J.; Sella, A.; Corà, F.; Firth, S.; Darr, J. A.; McMillan, P. F. H2 and O2 Evolution from Water Half-Splitting Reactions by Graphitic Carbon Nitride Materials. *J. Phys. Chem. C* **2013**, *117* (14), 7178–7185.

(36) Wang, X.; Blechert, S.; Antonietti, M. Polymeric Graphitic Carbon Nitride for Heterogeneous Photocatalysis. *ACS Catal.* **2012**, *2* (8), 1596–1606.

(37) Peng, R.; Liang, L.; Hood, Z. D.; Boulesbaa, A.; Puretzky, A.; Ievlev, A. V.; Come, J.; Ovchinnikova, O. S.; Wang, H.; Ma, C.; Chi, M.; Sumpter, B. G.; Wu, Z. In-Plane Heterojunctions Enable Multiphasic Two-Dimensional (2D) MoS2 Nanosheets As Efficient Photocatalysts for Hydrogen Evolution from Water Reduction. *ACS Catal.* **2016**, *6* (10), 6723–6729.

(38) Qi, Y.; Xu, Q.; Wang, Y.; Yan, B.; Ren, Y.; Chen, Z. CO2-Induced Phase Engineering: Protocol for Enhanced Photoelectrocatalytic Performance of 2D MoS2 Nanosheets. *ACS Nano* **2016**, *10* (2), 2903–2909.

(39) Mahler, B.; Hoepfner, V.; Liao, K.; Ozin, G. A. Colloidal Synthesis of 1T-WS2 and 2H-WS2 Nanosheets: Applications for Photocatalytic Hydrogen Evolution. *J. Am. Chem. Soc.* **2014**, *136* (40), 14121–14127.

(40) Andoshe, D. M.; Jeon, J.-M.; Kim, S. Y.; Jang, H. W. Two-Dimensional Transition Metal Dichalcogenide Nanomaterials for Solar Water Splitting. *Electron. Mater. Lett.* **2015**, *11* (3), 323–335.

(41) Zhang, Q.; Wang, W.; Zhang, J.; Zhu, X.; Zhang, Q.; Zhang, Y.; Ren, Z.; Song, S.; Wang, J.; Ying, Z.; Wang, R.; Qiu, X.; Peng, T.; Fu, L. Highly Efficient Photocatalytic Hydrogen Evolution by ReS 2 via a Two-Electron Catalytic Reaction. *Adv. Mater.* **2018**, *30* (23), 1707123.

(42) Liu, H.; Xu, B.; Liu, J. M.; Yin, J.; Miao, F.; Duan, C. G.; Wan, X. G. Highly Efficient and Ultrastable Visible-Light Photocatalytic Water Splitting over ReS2. *Phys. Chem. Chem. Phys.* **2016**, *18* (21), 14222–14227.

(43) Ida, S.; Ishihara, T. Recent Progress in Two-Dimensional Oxide Photocatalysts for Water Splitting. *J. Phys. Chem. Lett.* **2014**, *5* (15), 2533–2542.

(44) Abe, R.; Shinohara, K.; Tanaka, A.; Hara, M.; Kondo, J. N.; Domen, K. Preparation of Porous Niobium Oxides by Soft-Chemical Process and Their Photocatalytic Activity. *Chem. Mater.* **1997**, *9* (10), 2179–2184.

(45) Comptons, O. C.; Mullet, C. H.; Chiang, S.; Osterloh, F. E. A Building Block Approach to Photochemical Water-Splitting Catalysts Based on Layered Niobate Nanosheets. *J. Phys. Chem. C* **2008**, *112* (15), 6202–6208.

(46) Rahman, M. Z.; Kwong, C. W.; Davey, K.; Qiao, S. Z. 2D Phosphorene as a Water Splitting Photocatalyst: Fundamentals to Applications. *Energy Environ. Sci.* **2016**, *9* (3), 709–728.

(47) Zhu, M.; Osakada, Y.; Kim, S.; Fujitsuka, M.; Majima, T. Black Phosphorus: A Promising Two Dimensional Visible and near-Infrared-Activated Photocatalyst for Hydrogen Evolution. *Appl. Catal. B Environ.* **2017**, *217*, 285–292.

(48) Hu, W.; Lin, L.; Zhang, R.; Yang, C.; Yang, J. Highly Efficient Photocatalytic Water Splitting over Edge-Modified Phosphorene Nanoribbons. *J. Am. Chem. Soc.* **2017**, *139* (43), 15429–15436.

(49) Sa, B.; Li, Y. L.; Qi, J.; Ahuja, R.; Sun, Z. Strain Engineering for Phosphorene: The Potential Application as a Photocatalyst. *J. Phys. Chem. C* **2014**, *118* (46), 26560–26568.

(50) Rupp, C. J.; Chakraborty, S.; Anversa, J.; Baierle, R. J.; Ahuja, R. Rationalizing the Hydrogen and Oxygen Evolution Reaction Activity of Two-Dimensional Hydrogenated Silicene and Germanene. *ACS Appl. Mater. Interfaces* **2016**, *8* (2), 1536–1544.

(51) Guo, Z.; Zhou, J.; Zhu, L.; Sun, Z. MXene: A

Promising Photocatalyst for Water Splitting. *J. Mater. Chem. A* **2016**, *4* (29), 11446–11452.

(52) Liu, J.; Li, X. B.; Wang, D.; Liu, H.; Peng, P.; Liu, L. M. Single-Layer Group-IVB Nitride Halides as Promising Photocatalysts. *J. Mater. Chem. A* **2014**, *2* (19), 6755–6761.

(53) Zhou, J.; Sumpter, B. G.; Kent, P. R. C.; Huang, J. A Novel and Functional Single-Layer Sheet of ZnSe. *ACS Appl. Mater. Interfaces* **2015**, *7* (3), 1458–1464.

(54) Sun, Y.; Sun, Z.; Gao, S.; Cheng, H.; Liu, Q.; Piao, J.; Yao, T.; Wu, C.; Hu, S.; Wei, S.; Xie, Y. Fabrication of Flexible and Freestanding Zinc Chalcogenide Single Layers. *Nat. Commun.* **2012**, *3* (1), 1057.

(55) Peng, Q.; Xiong, R.; Sa, B.; Zhou, J.; Wen, C.; Wu, B.; Anpo, M.; Sun, Z. Computational Mining of Photocatalysts for Water Splitting Hydrogen Production: Two-Dimensional InSe-Family Monolayers. *Catal. Sci. Technol.* **2017**, *7* (13), 2744–2752.

(56) Cui, Y.; Peng, L.; Sun, L.; Qian, Q.; Huang, Y. Two-Dimensional Few-Layer Group-III Metal Monochalcogenides as Effective Photocatalysts for Overall Water Splitting in the Visible Range. *J. Mater. Chem. A* **2018**, *6* (45), 22768–22777.

(57) Zhuang, H. L.; Hennig, R. G. Single-Layer Group-III Monochalcogenide Photocatalysts for Water Splitting. *Chem. Mater.* **2013**, *25* (15), 3232–3238.

(58) Zappia, M. I.; Bianca, G.; Bellani, S.; Serri, M.; Najafi, L.; Oropesa-Nuñez, R.; Martín-García, B.; Bouša, D.; Sedmidubský, D.; Pellegrini, V.; Sofer, Z.; Cupolillo, A.; Bonaccorso, F. Solution-Processed GaSe Nanoflake-Based Films for Photoelectrochemical Water Splitting and Photoelectrochemical-Type Photodetectors. *Adv. Funct. Mater.* **2020**, *30* (10), 1909572.

(59) Kishore, M. R. A.; Ravindran, P. Te Doped Indium (II) Selenide Photocatalyst for Water Splitting: A First Principles Study. In *AIP Conference Proceedings*; 2017; Vol. 1832.

(60) Li, Z.; Qiao, H.; Guo, Z.; Ren, X.; Huang, Z.; Qi, X.; Dhanabalan, S. C.; Ponraj, J. S.; Zhang, D.; Li, J.; Zhao, J.; Zhong, J.; Zhang, H. High-Performance Photo-Electrochemical Photodetector Based on Liquid-Exfoliated Few-Layered InSe Nanosheets with Enhanced Stability. *Adv. Funct. Mater.* **2018**, *28* (16), 1705237.

(61) Chowdhury, C.; Karmakar, S.; Datta, A. Monolayer Group IV-VI Monochalcogenides: Low-Dimensional Materials for Photocatalytic Water Splitting. *J. Phys. Chem. C* **2017**, *121* (14), 7615–7624.

(62) Lv, X.; Wei, W.; Sun, Q.; Li, F.; Huang, B.; Dai, Y. Two-Dimensional Germanium Monochalcogenides for Photocatalytic Water Splitting with High Carrier Mobility. *Appl. Catal. B Environ.* **2017**, *217*, 275–284.

(63) Sun, L.; Cui, Y.; Peng, L.; Du, J.; Wang, S.; Huang, Y. Two-Dimensional Blue-Phosphorene-Phase Germanium Monochalcogenide Photocatalysts for Water Splitting: From Ultraviolet to Visible Absorption. *J. Catal.* **2019**, *373*, 67–74.

(64) Qiao, M.; Chen, Y.; Wang, Y.; Li, Y. The Germanium Telluride Monolayer: A Two Dimensional Semiconductor with High Carrier Mobility for Photocatalytic Water Splitting. *J. Mater. Chem. A* **2018**, *6* (9), 4119–4125.

(65) Ji, Y.; Yang, M.; Dong, H.; Hou, T.; Wang, L.; Li, Y. Two-Dimensional Germanium Monochalcogenide Photocatalyst for Water Splitting under Ultraviolet, Visible to near-Infrared Light. *Nanoscale* **2017**, *9* (25), 8608–8615.

(66) Zhu, Y. L.; Yuan, J. H.; Song, Y. Q.; Wang, S.; Xue, K. H.; Xu, M.; Cheng, X. M.; Miao, X. S. Two-Dimensional Silicon Chalcogenides with High Carrier Mobility for Photocatalytic Water Splitting. *J. Mater. Sci.* **2019**, *54* (17), 11485–11496.

(67) Li, X.; Zuo, X.; Jiang, X.; Li, D.; Cui, B.; Liu, D. Enhanced Photocatalysis for Water Splitting in Layered Tin Chalcogenides with High Carrier Mobility. *Phys. Chem. Chem. Phys.* **2019**, *21* (14), 7559–7566.

(68) Ye, Y.; Guo, Q.; Liu, X.; Liu, C.; Wang, J.; Liu, Y.; Qiu, J. Two-Dimensional GeSe as an Isostructural and Isoelectronic Analogue of Phosphorene: Sonication-Assisted Synthesis, Chemical Stability, and Optical Properties. *Chem. Mater.* **2017**, *29* (19), 8361–8368.

(69) Wu, M.; Wei, S.-H.; Huang, L. Origin of Polymorphism of the Two-Dimensional Group-IV Monochalcogenides. *Phys. Rev. B* **2017**, *96* (20), 205411.

(70) Singh, A. K.; Hennig, R. G. Computational Prediction of Two-Dimensional Group-IV Mono-Chalcogenides. *Appl. Phys. Lett.* **2014**, *105* (4), 042103.

(71) Gomes, L. C.; Carvalho, A. Phosphorene Analogues: Isoelectronic Two-Dimensional Group-IV Monochalcogenides with Orthorhombic Structure. *Phys. Rev. B* **2015**, *92* (8), 085406.

(72) Zhu, Z.; Guan, J.; Liu, D.; Tománek, D. Designing Isoelectronic Counterparts to Layered Group V Semiconductors. *ACS Nano* **2015**, *9* (8), 8284–8290.

(73) Pletikosić, I.; von Rohr, F.; Pervan, P.; Das, P. K.; Vobornik, I.; Cava, R. J.; Valla, T. Band Structure of the IV-VI Black Phosphorus Analog and Thermoelectric SnSe. *Phys. Rev. Lett.* **2018**, *120* (15), 156403.

(74) Kamal, C.; Chakrabarti, A.; Ezawa, M. Direct Band Gaps in Group IV-VI Monolayer Materials: Binary Counterparts of Phosphorene. *Phys. Rev. B* **2016**, *93* (12), 125428.

(75) He, H.; Orlando, R.; Blanco, M. A.; Pandey, R.; Amzallag, E.; Baraille, I.; Rérat, M. First-Principles Study of the Structural, Electronic, and Optical Properties of Ga2O3 in its monoclinic and hxagonal phases. *Rev. B* **2006**, *74* (19), 195123.

(76) Gu, D.; Tao, X.; Chen, H.; Zhu, W.; Ouyang, Y.; Peng, Q. Enhanced Photocatalytic Activity for Water Splitting of Blue-Phase GeS and GeSe Monolayers via Biaxial Straining. *Nanoscale* **2019**, *11* (5), 2335–2342.

(77) Yang, J. H.; Zhang, Y.; Yin, W. J.; Gong, X. G.; Yakobson, B. I.; Wei, S. H. Two-Dimensional SiS Layers with Promising Electronic and Optoelectronic

Properties: Theoretical Prediction. *Nano Lett.* **2016**, *16* (2), 1110–1117.

(78) Wiedemeier, H.; Csillag, F. J. The Thermal Expansion and High Temperature Transformation of SnS and SnSe. *Zeitschrift fur Krist. - New Cryst. Struct.* **1979**, *149* (1–2), 17–29.

(79) Dewandre, A.; Hellman, O.; Bhattacharya, S.; Romero, A. H.; Madsen, G. K. H.; Verstraete, M. J. Two-Step Phase Transition in SnSe and the Origins of Its High Power Factor from First Principles. *Phys. Rev. Lett.* **2016**, *117* (27), 276601.

(80) Zhao, L.-D.; Lo, S.-H.; Zhang, Y.; Sun, H.; Tan, G.; Uher, C.; Wolverton, C.; Dravid, V. P.; Kanatzidis, M. G. Ultralow Thermal Conductivity and High Thermoelectric Figure of Merit in SnSe Crystals. *Nature* **2014**, *508* (7496), 373–377.

(81) Ul Haq, B.; AlFaify, S.; Laref, A.; Ahmed, R.; M. Taib, M. F. Dimensionality Reduction of Germanium Selenide for High-Efficiency Thermoelectric Applications. *Ceram. Int.* **2019**, *45* (12), 15122–15127.

(82) Zhou, X.; Hu, X.; Zhou, S.; Zhang, Q.; Li, H.; Zhai, T. Ultrathin 2D GeSe 2 Rhombic Flakes with High Anisotropy Realized by Van Der Waals Epitaxy. *Adv. Funct. Mater.* **2017**, *27* (47), 1703858.

(83) von Rohr, F. O.; Ji, H.; Cevallos, F. A.; Gao, T.; Ong, N. P.; Cava, R. J. High-Pressure Synthesis and Characterization of β-GeSe—A Six-Membered-Ring Semiconductor in an Uncommon Boat Conformation. *J. Am. Chem. Soc.* **2017**, *139* (7), 2771–2777.

(84) Zhou, J.; Zhang, S.; Li, J. Normal-to-Topological Insulator Martensitic Phase Transition in Group-IV Monochalcogenides Driven by Light. *NPG Asia Mater.* **2020**, *12* (1), 2.

(85) Wang, Z.; Wang, J.; Zang, Y.; Zhang, Q.; Shi, J.-A.; Jiang, T.; Gong, Y.; Song, C.-L.; Ji, S.-H.; Wang, L.-L.; Gu, L.; He, K.; Duan, W.; Ma, X.; Chen, X.; Xue, Q.-K. Molecular Beam Epitaxy-Grown SnSe in the Rock-Salt Structure: An Artificial Topological Crystalline Insulator Material. *Adv. Mater.* **2015**, *27* (28), 4150–4154.

(86) Hu, Z.-Y.; Li, K.-Y.; Lu, Y.; Huang, Y.; Shao, X.-H. High Thermoelectric Performances of Monolayer SnSe Allotropes. *Nanoscale* **2017**, *9* (41), 16093–16100.

(87) Zhang, S.; Liu, S.; Huang, S.; Cai, B.; Xie, M.; Qu, L.; Zou, Y.; Hu, Z.; Yu, X.; Zeng, H. Structural and Electronic Properties of Atomically Thin Germanium Selenide Polymorphs. *Sci. China Mater.* **2015**, *58* (12), 929–935.

(88) Hu, T.; Dong, J. Two New Phases of Monolayer Group-IV Monochalcogenides and Their Piezoelectric Properties. *Phys. Chem. Chem. Phys.* **2016**, *18* (47), 32514–32520.

(89) Kagdada, H. L.; Jha, P. K.; Śpiewak, P.; Kurzydłowski, K. J.; Singh, D. K. Pressure-Induced First Order Phase Transition in Bulk GeSe. *J. Appl. Phys.* **2020**, *127* (17), 175104.

(90) Hu, Z.; Ding, Y.; Hu, X.; Zhou, W.; Yu, X.; Zhang, S. Recent Progress in 2D Group IV–IV Monochalcogenides: Synthesis, Properties and Applications. *Nanotechnology* **2019**, *30* (25), 252001.

(91) Hu, Y.; Zhang, S.; Sun, S.; Xie, M.; Cai, B.; Zeng, H. GeSe Monolayer Semiconductor with Tunable Direct Band Gap and Small Carrier Effective Mass. *Appl. Phys. Lett.* **2015**, *107* (12), 122107.

(92) Fan, Z.-Q.; Jiang, X.-W.; Wei, Z.; Luo, J.-W.; Li, S.-S. Tunable Electronic Structures of GeSe Nanosheets and Nanoribbons. *J. Phys. Chem. C* **2017**, *121* (26), 14373–14379.

(93) Nguyen, H. T. T.; Vu, T. V.; Binh, N. T. T.; Hoat, D. M.; Hieu, N. V.; Anh, N. T. T.; Nguyen, C. V.; Phuc, H. V.; Jappor, H. R.; Obeid, M. M.; Hieu, N. N. Strain-Tunable Electronic and Optical Properties of Monolayer GeSe: Promising for Photocatalytic Water Splitting Applications. *Chem. Phys.* **2020**, *529*, 110543.

(94) Huang, L.; Wu, F.; Li, J. Structural Anisotropy Results in Strain-Tunable Electronic and Optical Properties in Monolayer GeX and SnX (X = S, Se, Te). *J. Chem. Phys.* **2016**, *144* (11), 114708.

(95) Zhao, P.; Yang, H.; Li, J.; Jin, H.; Wei, W.; Yu, L.; Huang, B.; Dai, Y. Design of New Photovoltaic Systems Based on Two-Dimensional Group-IV Monochalcogenides for High Performance Solar Cells. *J. Mater. Chem. A* **2017**, *5* (46), 24145–24152.

(96) Xue, D. J.; Liu, S. C.; Dai, C. M.; Chen, S.; He, C.; Zhao, L.; Hu, J. S.; Wan, L. J. GeSe Thin-Film Solar Cells Fabricated by Self-Regulated Rapid Thermal Sublimation. *J. Am. Chem. Soc.* **2017**, *139* (2), 958–965. 5.

(97) Liu, S. C.; Mi, Y.; Xue, D. J.; Chen, Y. X.; He, C.; Liu, X.; Hu, J. S.; Wan, L. J. Investigation of Physical and Electronic Properties of GeSe for Photovoltaic Applications. *Adv. Electron. Mater.* **2017**, *3* (11), 1700141.

(98) Cook, A. M.; M. Fregoso, B.; de Juan, F.; Coh, S.; Moore, J. E. Design Principles for Shift Current Photovoltaics. *Nat. Commun.* **2017**, *8* (1), 14176.

(99) Mukherjee, B.; Cai, Y.; Tan, H. R.; Feng, Y. P.; Tok, E. S.; Sow, C. H. NIR Schottky Photodetectors Based on Individual Single-Crystalline GeSe Nanosheet. *ACS Appl. Mater. Interfaces* **2013**, *5* (19), 9594–9604.

(100) Xue, D.-J.; Tan, J.; Hu, J.-S.; Hu, W.; Guo, Y.-G.; Wan, L.-J. Anisotropic Photoresponse Properties of Single Micrometer-Sized GeSe Nanosheet. *Adv. Mater.* **2012**, *24* (33), 4528–4533.

(101) Ramasamy, P.; Kwak, D.; Lim, D.-H.; Ra, H.-S.; Lee, J.-S. Solution Synthesis of GeS and GeSe Nanosheets for High-Sensitivity Photodetectors. *J. Mater. Chem. C* **2016**, *4* (3), 479–485.

(102) Ma, D.; Zhao, J.; Wang, R.; Xing, C.; Li, Z.; Huang, W.; Jiang, X.; Guo, Z.; Luo, Z.; Li, Y.; Li, J.; Luo, S.; Zhang, Y.; Zhang, H. Ultrathin GeSe Nanosheets: From Systematic Synthesis to Studies of Carrier Dynamics and Applications for a High-Performance UV–Vis Photodetector. *ACS Appl. Mater. Interfaces* **2019**, *11* (4), 4278–4287.

(103) Tan, D.; Wang, X.; Zhang, W.; Lim, H. E.; Shinokita, K.; Miyauchi, Y.; Maruyama, M.; Okada, S.; Matsuda, K. Carrier Transport and Photoresponse in GeSe/MoS

2 Heterojunction p–n Diodes. *Small* **2018**, *14* (22), 1704559.

(104) Zhou, X.; Hu, X.; Jin, B.; Yu, J.; Liu, K.; Li, H.; Zhai, T. Highly Anisotropic GeSe Nanosheets for Phototransistors with Ultrahigh Photoresponsivity. *Adv. Sci.* **2018**, *5* (8), 1800478.

(105) Hu, X.; Huang, P.; Liu, K.; Jin, B.; Zhang, X.; Zhang, X.; Zhou, X.; Zhai, T. Salt-Assisted Growth of Ultrathin GeSe Rectangular Flakes for Phototransistors with Ultrahigh Responsivity. *ACS Appl. Mater. Interfaces* **2019**, *11* (26), 23353–23360.

(106) Brahma, M.; Kabiraj, A.; Saha, D.; Mahapatra, S. Scalability Assessment of Group-IV Mono-Chalcogenide Based Tunnel FET. *Sci. Rep.* **2018**, *8* (1), 5993.

(107) Kang, S.-Y.; Yoon, Y.-S.; Park, N.-W.; Lee, W.-Y.; Kim, G.-S.; Yoon, Y.-G.; Koh, J.-H.; Koo, S.-M.; Umar, A.; Lee, S.-K. Electrical Properties of Exfoliated Multilayer Germanium Selenide (GeSe) Nanoflake Field-Effect Transistors. *Sci. Adv. Mater.* **2018**, *10* (11), 1596–1600.

(108) Yap, W. C.; Yang, Z.; Mehboudi, M.; Yan, J. A.; Barraza-Lopez, S.; Zhu, W. Layered Material GeSe and Vertical GeSe/MoS2 p-n Heterojunctions. *Nano Res.* **2018**, *11* (1), 420–430.

(109) Alhazmi, A.; Amer, M. R. Electron Transport Performance of Germanium Selenide and Germanium Sulfide Field-Effect-Transistors in Dual Gates Configuration. In *2018 IEEE 18th International Conference on Nanotechnology (IEEE-NANO)*; IEEE, 2018; pp 1–1.

(110) Liu, C.; Guan, S.; Yin, H.; Wan, W.; Wang, Y.; Zhang, Y. γ-GeSe: A Two-Dimensional Ferroelectric Material with Doping-Induced Ferromagnetism. *Appl. Phys. Lett.* **2019**, *115* (25), 252904.

(111) Li, Z.; Liu, M.; Chen, Q.; Huang, Y.; Cao, C.; He, Y. The Electronic Structure of GeSe Monolayer with Light Nonmetallic Elements Decoration. *Superlattices Microstruct.* **2017**, *109*, 829–840.

(112) Fei, R.; Li, W.; Li, J.; Yang, L. Giant Piezoelectricity of Monolayer Group IV Monochalcogenides: SnSe, SnS, GeSe, and GeS. *Appl. Phys. Lett.* **2015**, *107* (17), 173104.

(113) Fei, R.; Kang, W.; Yang, L. Ferroelectricity and Phase Transitions in Monolayer Group-IV Monochalcogenides. *Phys. Rev. Lett.* **2016**, *117* (9), 097601.

(114) Zhou, Y.; Zhao, M.; Chen, Z. W.; Shi, X. M.; Jiang, Q. Potential Application of 2D Monolayer β-GeSe as an Anode Material in Na/K Ion Batteries. *Phys. Chem. Chem. Phys.* **2018**, *20* (48), 30290–30296.

(115) He, C.; Zhang, J. H.; Zhang, W. X.; Li, T. T. GeSe/BP van Der Waals Heterostructures as Promising Anode Materials for Potassium-Ion Batteries. *J. Phys. Chem. C* **2019**, *123* (9), 5157–5163.

(116) Sannyal, A.; Zhang, Z.; Gao, X.; Jang, J. Two-Dimensional Sheet of Germanium Selenide as an Anode Material for Sodium and Potassium Ion Batteries: First-Principles Simulation Study. *Comput. Mater. Sci.* **2018**, *154*, 204–211.

(117) Zhou, Y. MX (M = Ge, Sn; X = S, Se) Sheets: Theoretical Prediction of New Promising Electrode Materials for Li Ion Batteries. *J. Mater. Chem. A* **2016**, *4* (28), 10906–10913.

(118) Zacharia, R.; Ulbricht, H.; Hertel, T. Interlayer Cohesive Energy of Graphite from Thermal Desorption of Polyaromatic Hydrocarbons. *Phys. Rev. B - Condens. Matter Mater. Phys.* **2004**, *69* (15).

(119) Ziambaras, E.; Kleis, J.; Schröder, E.; Hyldgaard, P. Potassium Intercalation in Graphite: A van Der Waals Density-Functional Study. *Phys. Rev. B - Condens. Matter Mater. Phys.* **2007**, *76* (15), 155425.

(120) Wang, W.; Dai, S.; Li, X.; Yang, J.; Srolovitz, D. J.; Zheng, Q. Measurement of the Cleavage Energy of Graphite. *Nat. Commun.* **2015**, *6* (1), 7853.

(121) Björkman, T.; Gulans, A.; Krasheninnikov, A. V; Nieminen, R. M. Van Der Waals Bonding in Layered Compounds from Advanced Density-Functional First-Principles Calculations. *Phys. Rev. Lett.* **2012**, *108* (23), 235502.

(122) Schusteritsch, G.; Uhrin, M.; Pickard, C. J. Single-Layered Hittorf's Phosphorus: A Wide-Bandgap High Mobility 2D Material. *Nano Lett.* **2016**, *16* (5), 2975–2980.

(123) Shulenburger, L.; Baczewski, A. D.; Zhu, Z.; Guan, J.; Tománek, D. The Nature of the Interlayer Interaction in Bulk and Few-Layer Phosphorus. *Nano Lett.* **2015**, *15* (12), 8170–8175.

(124) Bonaccorso, F.; Lombardo, A.; Hasan, T.; Sun, Z.; Colombo, L.; Ferrari, A. C. Production and Processing of Graphene and 2d Crystals. *Mater. Today* **2012**, *15* (12), 564–589.

(125) Yi, M.; Shen, Z. A Review on Mechanical Exfoliation for the Scalable Production of Graphene. *J. Mater. Chem. A* **2015**, *3* (22), 11700–11715.

(126) Magda, G. Z.; Pető, J.; Dobrik, G.; Hwang, C.; Biró, L. P.; Tapasztó, L. Exfoliation of Large-Area Transition Metal Chalcogenide Single Layers. *Sci. Rep.* **2015**, *5* (1), 14714.

(127) Bonaccorso, F.; Bartolotta, A.; Coleman, J. N.; Backes, C. 2D-Crystal-Based Functional Inks. *Adv. Mater.* **2016**, *28* (29), 6136–6166.

(128) Del Rio Castillo, A. E.; Pellegrini, V.; Ansaldo, A.; Ricciardella, F.; Sun, H.; Marasco, L.; Buha, J.; Dang, Z.; Gagliani, L.; Lago, E.; Curreli, N.; Gentiluomo, S.; Palazon, F.; Prato, M.; Oropesa-Nuñez, R.; Toth, P. S.; Mantero, E.; Crugliano, M.; Gamucci, A.; Tomadin, A.; Polini, M.; Bonaccorso, F. High-Yield Production of 2D Crystals by Wet-Jet Milling. *Mater. Horizons* **2018**, *5* (5), 890–904.

(129) Bellani, S.; Petroni, E.; Del Rio Castillo, A. E.; Curreli, N.; Martín-García, B.; Oropesa-Nuñez, R.; Prato, M.; Bonaccorso, F. Scalable Production of Graphene Inks via Wet-Jet Milling Exfoliation for Screen-Printed Micro-Supercapacitors. *Adv. Funct. Mater.* **2019**, *29* (14), 1807659.

(130) Ribeiro, H. B.; Ramos, S. L. L. M.; Seixas, L.; de

Matos, C. J. S.; Pimenta, M. A. Edge Phonons in Layered Orthorhombic GeS and GeSe Monochalcogenides. *Phys. Rev. B* **2019**, *100* (9), 094301.

(131) Mao, Y.; Mao, X.; Zhao, H.; Zhang, N.; Shi, X.; Yuan, J. Enhancement of Photoluminescence Efficiency in GeSe Ultrathin Slab by Thermal Treatment and Annealing: Experiment and First-Principles Molecular Dynamics Simulations. *Sci. Rep.* **2018**, *8* (1), 17671.

(132) Gomes, L. C.; Carvalho, A.; Castro Neto, A. H. Vacancies and Oxidation of Two-Dimensional Group-IV Monochalcogenides. *Phys. Rev. B* **2016**, *94* (5), 054103.

(133) Guo, Y.; Zhou, S.; Bai, Y.; Zhao, J. Oxidation Resistance of Monolayer Group-IV Monochalcogenides. *ACS Appl. Mater. Interfaces* **2017**, *9* (13), 12013–12020.

(134) Favron, A.; Gaufrès, E.; Fossard, F.; Phaneuf-L'Heureux, A.-L.; Tang, N. Y. W.; Lévesque, P. L.; Loiseau, A.; Leonelli, R.; Francoeur, S.; Martel, R. Photooxidation and Quantum Confinement Effects in Exfoliated Black Phosphorus. *Nat. Mater.* **2015**, *14* (8), 826–832.

(135) Huang, Y.; Qiao, J.; He, K.; Bliznakov, S.; Sutter, E.; Chen, X.; Luo, D.; Meng, F.; Su, D.; Decker, J.; Ji, W.; Ruoff, R. S.; Sutter, P. Interaction of Black Phosphorus with Oxygen and Water. *Chem. Mater.* **2016**, *28* (22), 8330–8339.

(136) Ho, P. H.; Chang, Y. R.; Chu, Y. C.; Li, M. K.; Tsai, C. A.; Wang, W. H.; Ho, C. H.; Chen, C. W.; Chiu, P. W. High-Mobility InSe Transistors: The Role of Surface Oxides. *ACS Nano* **2017**, *11* (7), 7362–7370.

(137) Shi, L.; Zhou, Q.; Zhao, Y.; Ouyang, Y.; Ling, C.; Li, Q.; Wang, J. Oxidation Mechanism and Protection Strategy of Ultrathin Indium Selenide: Insight from Theory. *J. Phys. Chem. Lett.* **2017**, *8* (18), 4368–4373.

(138) Ma, D.; Li, T.; Yuan, D.; He, C.; Lu, Z.; Lu, Z.; Yang, Z.; Wang, Y. The Role of the Intrinsic Se and In Vacancies in the Interaction of O 2 and H 2 O Molecules with the InSe Monolayer. *Appl. Surf. Sci.* **2018**, *434*, 215–227.

(139) Kowalski, B. M.; Manz, N.; Bethke, D.; Shaner, E. A.; Serov, A.; Kalugin, N. G. Role of Humidity in Oxidation of Ultrathin GaSe. *Mater. Res. Express* **2019**, *6* (8), 085907.

(140) Bergeron, A.; Ibrahim, J.; Leonelli, R.; Francoeur, S. Oxidation Dynamics of Ultrathin GaSe Probed through Raman Spectroscopy. *Appl. Phys. Lett.* **2017**, *110* (24), 241901.

(141) Vaughn, D. D.; Patel, R. J.; Hickner, M. A.; Schaak, R. E. Single-Crystal Colloidal Nanosheets of GeS and GeSe. *J. Am. Chem. Soc.* **2010**, *132* (43), 15170–15172.

(142) Elkorashy, A. M. Photoconductivity in Germanium Selenide Single Crystals. *Phys. status solidi* **1989**, *152* (1), 249–259.

(143) Kannewurf, C. R.; Cashman, R. J. Optical Absorption and Photoconductivity in Germanium Selenide. *J. Phys. Chem. Solids* **1961**, *22*, 293–298.

(144) Kumara, A.; Ahluwalia, P. K. Electronic Structure of Transition Metal Dichalcogenides Monolayers 1H-MX2 (M = Mo, W; X = S, Se, Te) from Ab-Initio Theory: New Direct Band Gap Semiconductors. *Eur. Phys. J. B* **2012**, *85* (6), 186.

(145) Ellis, J. K.; Lucero, M. J.; Scuseria, G. E. The Indirect to Direct Band Gap Transition in Multilayered MoS2 as Predicted by Screened Hybrid Density Functional Theory. *Appl. Phys. Lett.* **2011**, *99* (26), 261908.

(146) Mak, K. F.; Lee, C.; Hone, J.; Shan, J.; Heinz, T. F. Atomically Thin MoS 2 : A New Direct-Gap Semiconductor. *Phys. Rev. Lett.* **2010**, *105* (13), 136805.

(147) Splendiani, A.; Sun, L.; Zhang, Y.; Li, T.; Kim, J.; Chim, C.-Y.; Galli, G.; Wang, F. Emerging Photoluminescence in Monolayer MoS2. *Nano Lett.* **2010**, *10* (4), 1271–1275.

(148) Zhang, Y.; Chang, T. R.; Zhou, B.; Cui, Y. T.; Yan, H.; Liu, Z.; Schmitt, F.; Lee, J.; Moore, R.; Chen, Y.; Lin, H.; Jeng, H. T.; Mo, S. K.; Hussain, Z.; Bansil, A.; Shen, Z. X. Direct Observation of the Transition from Indirect to Direct Bandgap in Atomically Thin Epitaxial MoSe2. *Nat. Nanotechnol.* **2014**, *9* (2), 111–115.

(149) Shi, G.; Kioupakis, E. Anisotropic Spin Transport and Strong Visible-Light Absorbance in Few-Layer SnSe and GeSe. *Nano Lett.* **2015**, *15* (10), 6926–6931.

(150) Yang, M.; Cao, S.; You, Q.; Shi, L. Bin; Qian, P. Intrinsic Carrier Mobility of Monolayer GeS and GeSe: First-Principles Calculation. *Phys. E Low-Dimensional Syst. Nanostructures* **2020**, *118*, 113877.

(151) Xu, Y.; Zhang, H.; Shao, H.; Ni, G.; Li, J.; Lu, H.; Zhang, R.; Peng, B.; Zhu, Y.; Zhu, H.; Soukoulis, C. M. First-Principles Study on the Electronic, Optical, and Transport Properties of Monolayer α- and β -GeSe. *Phys. Rev. B* **2017**, *96* (24), 245421.

(152) Shafique, A.; Shin, Y.-H. Thermoelectric and Phonon Transport Properties of Two-Dimensional IV–VI Compounds. *Sci. Rep.* **2017**, *7* (1), 506.

(153) Solanki, G. K.; Deshpande, M. P.; Agarwal, M. K.; Patel, P. D.; Vaidya, S. N. Thermoelectric Power Factor Measurements in GeSe Single Crystals Grown Using Different Transporting Agents. *J. Mater. Sci. Lett.* **2003**, *22* (14), 985–987.

(154) Tran, P. D.; Artero, V.; Fontecave, M. Water Electrolysis and Photoelectrolysis on Electrodes Engineered Using Biological and Bio-Inspired Molecular Systems. *Energy Environ. Sci.* **2010**, *3* (6), 727.

(155) Brlmblecombe, R.; Koo, A.; Dismukes, G. C.; Swlegers, G. F.; Spiccia, L. Solar Driven Water Oxidation by a Bioinspired Manganese Molecular Catalyst. *J. Am. Chem. Soc.* **2010**, *132* (9), 2892–2894.

(156) Zhou, P.; Yu, J.; Jaroniec, M. All-Solid-State Z-Scheme Photocatalytic Systems. *Adv. Mater.* **2014**, *26* (29), 4920–4935.

(157) Wang, W.; Chen, S.; Yang, P. X.; Duan, C. G.; Wang, L. W. Si:WO3 Heterostructure for Z-Scheme Water Splitting: An Ab Initio Study. *J. Mater. Chem. A* **2013**,

1 (4), 1078–1085.

(158) Kothe, T.; Plumeré, N.; Badura, A.; Nowaczyk, M. M.; Guschin, D. A.; Rögner, M.; Schuhmann, W. Combination of a Photosystem 1-Based Photocathode and a Photosystem 2-Based Photoanode to a z-Scheme Mimic for Biophotovoltaic Applications. *Angew. Chem. Int. Ed.* **2013**, *52* (52), 14233–14236.

(159) Peerakiatkhajohn, P.; Yun, J.-H.; Wang, S.; Wang, L. Review of Recent Progress in Unassisted Photoelectrochemical Water Splitting: From Material Modification to Configuration Design. *J. Photonics Energy* **2016**, *7* (1), 012006.

(160) Tachibana, Y.; Vayssieres, L.; Durrant, J. R. Artificial Photosynthesis for Solar Water-Splitting. *Nat. Photonics* **2012**, *6* (8), 511–518.

(161) Perdew, J. P.; Burke, K.; Ernzerhof, M. Generalized Gradient Approximation Made Simple. *Phys. Rev. Lett.* **1996**, *77* (18), 3865–3868.

(162) Heyd, J.; Scuseria, G. E.; Ernzerhof, M. Hybrid Functionals Based on a Screened Coulomb Potential. *J. Chem. Phys.* **2003**, *118* (18), 8207–8215.

(163) Galy, J.; Vignoles, G. L. The Role of P 3s2 Lone Pair (E) in Structure, Properties and Phase Transitions of Black Phosphorus. Stereochemistry and Ab Initio Topology Analyses. *Solid State Sci.* **2020**, *100*, 106068.

(164) Boukhvalov, D. W.; Rudenko, A. N.; Prishchenko, D. A.; Mazurenko, V. G.; Katsnelson, M. I. Chemical Modifications and Stability of Phosphorene with Impurities: A First Principles Study. *Phys. Chem. Chem. Phys.* **2015**, *17* (23), 15209–15217.

(165) Zhang, H.; Yang, G.; Zuo, X.; Tang, H.; Yang, Q.; Li, G. Computational Studies on the Structural, Electronic and Optical Properties of Graphene-like MXenes (M2CT2, M = Ti, Zr, Hf; T = O, F, OH) and Their Potential Applications as Visible-Light Driven Photocatalysts. *J. Mater. Chem. A* **2016**, *4* (33), 12913–12920.

(166) Novoselov, K. S.; Mishchenko, A.; Carvalho, A.; Castro Neto, A. H. 2D Materials and van Der Waals Heterostructures. *Science (80-.).* **2016**, *353* (6298), aac9439.

(167) Das, S.; Robinson, J. A.; Dubey, M.; Terrones, H.; Terrones, M. Beyond Graphene: Progress in Novel Two-Dimensional Materials and van Der Waals Solids. *Annu. Rev. Mater. Res.* **2015**, *45* (1), 1–27.

(168) Tan, S. M.; Chua, C. K.; Sedmidubský, D.; Sofer, Z.; Pumera, M. Electrochemistry of Layered GaSe and GeS: Applications to ORR, OER and HER. *Phys. Chem. Chem. Phys.* **2016**, *18* (3), 1699–1711.

(169) Dutta, S. N.; Jeffrey, G. A. On the Structure of Germanium Selenide and Related Binary IV/VI Compounds. *Inorg. Chem.* **1965**, *4* (9), 1363–1366.

(170) Schmeisser, D.; Schnell, R. D.; Bogen, A.; Himpsel, F. J.; Rieger, D.; Landgren, G.; Morar, J. F. Surface Oxidation States of Germanium. *Surf. Sci.* **1986**, *172* (2), 455–465.

(171) Prabhakaran, K.; Ogino, T. Oxidation of Ge(100) and Ge(111) Surfaces: An UPS and XPS Study. *Surf. Sci.* **1995**, *325* (3), 263–271.

(172) Lam, D.; Chen, K.-S.; Kang, J.; Liu, X.; Hersam, M. C. Anhydrous Liquid-Phase Exfoliation of Pristine Electrochemically Active GeS Nanosheets. *Chem. Mater.* **2018**, *30* (7), 2245–2250.

(173) Harvey, A.; Backes, C.; Gholamvand, Z.; Hanlon, D.; McAteer, D.; Nerl, H. C.; McGuire, E.; Seral-Ascaso, A.; Ramasse, Q. M.; McEvoy, N.; Winters, S.; Berner, N. C.; McCloskey, D.; Donegan, J. F.; Duesberg, G. S.; Nicolosi, V.; Coleman, J. N. Preparation of Gallium Sulfide Nanosheets by Liquid Exfoliation and Their Application As Hydrogen Evolution Catalysts. *Chem. Mater.* **2015**, *27* (9), 3483–3493.

(174) Petroni, E.; Lago, E.; Bellani, S.; Boukhvalov, D. W.; Politano, A.; Gürbulak, B.; Duman, S.; Prato, M.; Gentiluomo, S.; Oropesa-Nuñez, R.; Panda, J.-K.; Toth, P. S.; Del Rio Castillo, A. E.; Pellegrini, V.; Bonaccorso, F. Liquid-Phase Exfoliated Indium–Selenide Flakes and Their Application in Hydrogen Evolution Reaction. *Small* **2018**, *14* (26), 1800749.

(175) Curreli, N.; Serri, M.; Spirito, D.; Lago, E.; Petroni, E.; Martín-García, B.; Politano, A.; Gürbulak, B.; Duman, S.; Krahne, R.; Pellegrini, V.; Bonaccorso, F. Liquid Phase Exfoliated Indium Selenide Based Highly Sensitive Photodetectors. *Adv. Funct. Mater.* **2020**, *30* (13), 1908427.

(176) Najafi, L.; Bellani, S.; Martín-García, B.; Oropesa-Nuñez, R.; Del Rio Castillo, A. E.; Prato, M.; Moreels, I.; Bonaccorso, F. Solution-Processed Hybrid Graphene Flake/2H-MoS2 Quantum Dot Heterostructures for Efficient Electrochemical Hydrogen Evolution. *Chem. Mater.* **2017**, *29* (14), 5782–5786.

(177) Najafi, L.; Bellani, S.; Oropesa-Nuñez, R.; Ansaldo, A.; Prato, M.; Del Rio Castillo, A. E.; Bonaccorso, F. Doped-MoSe2 Nanoflakes/3d Metal Oxide–Hydr(Oxy)Oxides Hybrid Catalysts for PH-Universal Electrochemical Hydrogen Evolution Reaction. *Adv. Energy Mater.* **2018**, *8* (27), 1801764.

(178) Bellani, S.; Martín-García, B.; Oropesa-Nuñez, R.; Romano, V.; Najafi, L.; Demirci, C.; Prato, M.; Del Rio Castillo, A. E.; Marasco, L.; Mantero, E.; D'Angelo, G.; Bonaccorso, F. "Ion Sliding" on Graphene: A Novel Concept to Boost Supercapacitor Performance. *Nanoscale Horizons* **2019**, *4* (5), 1077–1091.

(179) Ansaldo, A.; Bondavalli, P.; Bellani, S.; Del Rio Castillo, A. E.; Prato, M.; Pellegrini, V.; Pognon, G.; Bonaccorso, F. High-Power Graphene–Carbon Nanotube Hybrid Supercapacitors. *ChemNanoMat* **2017**, *3* (6), 436–446.

(180) Jawaid, A.; Nepal, D.; Park, K.; Jespersen, M.; Qualley, A.; Mirau, P.; Drummy, L. F.; Vaia, R. A. Mechanism for Liquid Phase Exfoliation of MoS2. *Chem. Mater.* **2016**, *28* (1), 337–348.

(181) Capasso, A.; Matteocci, F.; Najafi, L.; Prato, M.; Buha, J.; Cinà, L.; Pellegrini, V.; Carlo, A. Di; Bonaccorso, F. Few-Layer MoS2 Flakes as Active Buffer Layer for Stable Perovskite Solar Cells. *Adv. Energy Mater.* **2016**, *6* (16), 1600920.

(182) Tsikritzis, D.; Rogdakis, K.; Chatzimanolis, K.; Petrović, M.; Tzoganakis, N.; Najafi, L.; Martín-

García, B.; Oropesa-Nuñez, R.; Bellani, S.; Del Rio Castillo, A. E.; Prato, M.; Stylianakis, M. M.; Bonaccorso, F.; Kymakis, E. A Two-Fold Engineering Approach Based on Bi 2 Te 3 Flakes towards Efficient and Stable Inverted Perovskite Solar Cells. *Mater. Adv.* **2020**, *1* (3), 450–462.

(183) Kang, J.; Sangwan, V. K.; Wood, J. D.; Hersam, M. C. Solution-Based Processing of Monodisperse Two-Dimensional Nanomaterials. *Acc. Chem. Res.* **2017**, *50* (4), 943–951.

(184) Najafi, L.; Bellani, S.; Oropesa-Nuñez, R.; Ansaldo, A.; Prato, M.; Del Rio Castillo, A. E.; Bonaccorso, F. Engineered MoSe2-Based Heterostructures for Efficient Electrochemical Hydrogen Evolution Reaction. *Adv. Energy Mater.* **2018**, *8* (16), 1703212.

(185) Najafi, L.; Oropesa-Nuñez, R.; Martín-García, B.; Drago, F.; Prato, M.; Pellegrini, V.; Bonaccorso, F.; Bellani, S. Water-Dispersible Few-Layer Graphene Flakes for Selective and Rapid Ion Mercury (Hg 2+)-Rejecting Membranes. *Mater. Adv.* **2020**, *1* (3), 387–402.

(186) Zhao, H.; Mao, Y.; Mao, X.; Shi, X.; Xu, C.; Wang, C.; Zhang, S.; Zhou, D. Band Structure and Photoelectric Characterization of GeSe Monolayers. *Adv. Funct. Mater.* **2018**, *28*, 1704855.

(187) Wiedemeier, H.; Schnering, H. G. Von. Refinement of the Structures of GeS, GeSe, SnS and SnSe. *Zeitschrift fur Krist. - New Cryst. Struct.* **1978**, *148* (3–4), 295–303.

(188) Chandrasekhar, H. R.; Zwick, U. Raman Scattering and Infrared Reflectivity in GeSe. *Solid State Commun.* **1976**, *18* (11–12), 1509–1513.

(189) Fukunaga, T.; Sugai, S.; Kinosada, T.; Murase, K. Observation of New Raman Lines in GeSe and SnSe at Low Temperatures. *Solid State Commun.* **1981**, *38* (11), 1049–1052.

(190) Zhang, X.; Tan, Q.-H.; Wu, J.-B.; Shi, W.; Tan, P.-H. Review on the Raman Spectroscopy of Different Types of Layered Materials. *Nanoscale* **2016**, *8* (12), 6435–6450.

(191) Taube, A.; Łapińska, A.; Judek, J.; Wochtman, N.; Zdrojek, M. Temperature Induced Phonon Behaviour in Germanium Selenide Thin Films Probed by Raman Spectroscopy. *J. Phys. D. Appl. Phys.* **2016**, *49* (31), 315301.

(192) Liu, J.; Zhou, Y.; Lin, Y.; Li, M.; Cai, H.; Liang, Y.; Liu, M.; Huang, Z.; Lai, F.; Huang, F.; Zheng, W. Anisotropic Photoresponse of the Ultrathin GeSe Nanoplates Grown by Rapid Physical Vapor Deposition. *ACS Appl. Mater. Interfaces* **2019**, *11* (4), 4123–4130.

(193) Feng, Y.; Zhou, J.; Du, Y.; Miao, F.; Duan, C.-G.; Wang, B.; Wan, X. Raman Spectra of Few-Layer Phosphorene Studied from First-Principles Calculations. *J. Phys. Condens. Matter* **2015**, *27* (18), 185302.

(194) Guo, Z.; Zhang, H.; Lu, S.; Wang, Z.; Tang, S.; Shao, J.; Sun, Z.; Xie, H.; Wang, H.; Yu, X.-F.; Chu, P. K. From Black Phosphorus to Phosphorene: Basic Solvent Exfoliation, Evolution of Raman Scattering, and Applications to Ultrafast Photonics. *Adv. Funct. Mater.* **2015**, *25* (45), 6996–7002.

(195) Ferrari, A. C.; Basko, D. M. Raman Spectroscopy as a Versatile Tool for Studying the Properties of Graphene. *Nat. Nanotechnol.* **2013**, *8* (4), 235–246.

(196) Bonaccorso, F.; Tan, P.-H.; Ferrari, A. C. Multiwall Nanotubes, Multilayers, and Hybrid Nanostructures: New Frontiers for Technology and Raman Spectroscopy. *ACS Nano* **2013**, *7* (3), 1838–1844.

(197) Najafi, L.; Bellani, S.; Oropesa-Nuñez, R.; Martín-García, B.; Prato, M.; Bonaccorso, F. Single-/Few-Layer Graphene as Long-Lasting Electrocatalyst for Hydrogen Evolution Reaction. *ACS Appl. Energy Mater.* **2019**, *2* (8), 5373–5379.

(198) Galeener, F. L.; Mikkelsen, J. C.; Geils, R. H.; Mosby, W. J. The Relative Raman Cross Sections of Vitreous SiO2 , GeO 2 , B 2 O 3 , and P 2 O 5. *Appl. Phys. Lett.* **1978**, *32* (1), 34–36.

(199) Durben, D. J.; Wolf, G. H. Raman Spectroscopic Study of the Pressure-Induced Coordination Change in GeO2 Glass. *Phys. Rev. B* **1991**, *43* (3), 2355–2363.

(200) Carroll, P. J.; Lannin, J. S. Raman Scattering of Amorphous Selenium Films. *Solid State Commun.* **1981**, *40* (1), 81–84.

(201) Yang, L.; Miklavcic, S. J. Revised Kubelka–Munk Theory III A General Theory of Light Propagation in Scattering and Absorptive Media. *J. Opt. Soc. Am. A* **2005**, *22* (9), 1866.

(202) Vargas, W. E.; Niklasson, G. A. Applicability Conditions of the Kubelka–Munk Theory. *Appl. Opt.* **1997**, *36* (22), 5580.

(203) Najafi, L.; Taheri, B.; Martín-García, B.; Bellani, S.; Di Girolamo, D.; Agresti, A.; Oropesa-Nunìez, R.; Pescetelli, S.; Vesce, L.; Calabrò, E.; Prato, M.; Del Rio Castillo, A. E.; Di Carlo, A.; Bonaccorso, F. MoS2 Quantum Dot/Graphene Hybrids for Advanced Interface Engineering of a CH3NH3PbI3 Perovskite Solar Cell with an Efficiency of over 20%. *ACS Nano* **2018**, *12* (11), 10736–10754.

(204) Antunez, P. D.; Torelli, D. A.; Yang, F.; Rabuffetti, F. A.; Lewis, N. S.; Brutchey, R. L. Low Temperature Solution-Phase Deposition of SnS Thin Films. *Chem. Mater.* **2014**, *26* (19), 5444–5446.

(205) Patel, M.; Chavda, A.; Mukhopadhyay, I.; Kim, J.; Ray, A. Nanostructured SnS with Inherent Anisotropic Optical Properties for High Photoactivity. *Nanoscale* **2016**, *8* (4), 2293–2303.

(206) Woomer, A. H.; Farnsworth, T. W.; Hu, J.; Wells, R. A.; Donley, C. L.; Warren, S. C. Phosphorene: Synthesis, Scale-Up, and Quantitative Optical Spectroscopy. *ACS Nano* **2015**, *9* (9), 8869–8884.

(207) Tomaszewska, E.; Soliwoda, K.; Kadziola, K.; Tkacz-Szczesna, B.; Celichowski, G.; Cichomski, M.; Szmaja, W.; Grobelny, J. Detection Limits of DLS and UV-Vis Spectroscopy in Characterization of Polydisperse Nanoparticles Colloids. *J. Nanomater.* **2013**, *2013*, 1–10.

(208) Hernandez, Y.; Nicolosi, V.; Lotya, M.; Blighe, F. M.;

Sun, Z.; De, S.; McGovern, I. T.; Holland, B.; Byrne, M.; Gun'Ko, Y. K.; Boland, J. J.; Niraj, P.; Duesberg, G.; Krishnamurthy, S.; Goodhue, R.; Hutchison, J.; Scardaci, V.; Ferrari, A. C.; Coleman, J. N. High-Yield Production of Graphene by Liquid-Phase Exfoliation of Graphite. *Nat. Nanotechnol.* **2008**, *3* (9), 563–568.

(209) Malacara, D. Color Vision and Colorimetry: Theory and Applications. *Color Res. Appl.* **2003**, *28* (1), 77–78.

(210) Cohen, J.; Wyszecki, G.; Stiles, W. S. Color Science: Concepts and Methods, Quantitative Data and Formulas. *Am. J. Psychol.* **1968**, *81* (1), 128.

(211) Antognazza, M. R.; Scherf, U.; Monti, P.; Lanzani, G. Organic-Based Tristimuli Colorimeter. *Appl. Phys. Lett.* **2007**, *90* (16), 163509.

(212) https://www.thorlabs.com/navigation.cfm?guide_id=36 (data accessed on 24/07/2020)

(213) Takata, T.; Jiang, J.; Sakata, Y.; Nakabayashi, M.; Shibata, N.; Nandal, V.; Seki, K.; Hisatomi, T.; Domen, K. Photocatalytic Water Splitting with a Quantum Efficiency of Almost Unity. *Nature* **2020**, *581* (7809), 411–414.

(214) Mauritz, K. A.; Moore, R. B. State of Understanding of Nafion. *Chem. Rev.* **2004**, *104* (10), 4535–4586.

(215) Zawodzinski, T. A. Water Uptake by and Transport Through Nafion® 117 Membranes. *J. Electrochem. Soc.* **1993**, *140* (4), 1041.

(216) Jiang, C.; Moniz, S. J. A.; Wang, A.; Zhang, T.; Tang, J. Photoelectrochemical Devices for Solar Water Splitting – Materials and Challenges. *Chem. Soc. Rev.* **2017**, *46* (15), 4645–4660.

(217) Joe, J.; Yang, H.; Bae, C.; Shin, H. Metal Chalcogenides on Silicon Photocathodes for Efficient Water Splitting: A Mini Overview. *Catalysts* **2019**, *9* (2), 149.

(218) McGlynn, S. P. Concepts in Photoconductivity and Allied Problems. *J. Am. Chem. Soc.* **1964**, *86* (24), 5707–5707.

(219) Guo, F.; Yang, B.; Yuan, Y.; Xiao, Z.; Dong, Q.; Bi, Y.; Huang, J. A Nanocomposite Ultraviolet Photodetector Based on Interfacial Trap-Controlled Charge Injection. *Nat. Nanotechnol.* **2012**, *7* (12), 798–802.

(220) Wang, H.; Zhang, X.; Xie, Y. Recent Progress in Ultrathin Two-Dimensional Semiconductors for Photocatalysis. *Mater. Sci. Eng. R Reports* **2018**, *130*, 1–39.

(221) Kong, D.; Cha, J. J.; Wang, H.; Lee, H. R.; Cui, Y. First-Row Transition Metal Dichalcogenide Catalysts for Hydrogen Evolution Reaction. *Energy Environ. Sci.* **2013**, *6* (12), 3553–3558.

(222) Yang, J.; Shin, H. S. Recent Advances in Layered Transition Metal Dichalcogenides for Hydrogen Evolution Reaction. *J. Mater. Chem. A* **2014**, *2* (17), 5979–5985.

(223) Najafi, L.; Bellani, S.; Oropesa-Nuñez, R.; Martín-García, B.; Prato, M.; Pasquale, L.; Panda, J. K.; Marvan, P.; Sofer, Z.; Bonaccorso, F. TaS2, TaSe2, and Their Heterogeneous Films as Catalysts for the Hydrogen Evolution Reaction. *ACS Catal.* **2020**, *10* (5), 3313–3325.

(224) Najafi, L.; Bellani, S.; Oropesa-Nuñez, R.; Martín-García, B.; Prato, M.; Mazánek, V.; Debellis, D.; Lauciello, S.; Brescia, R.; Sofer, Z.; Bonaccorso, F. Niobium Disulphide (NbS2)-Based (Heterogeneous) Electrocatalysts for an Efficient Hydrogen Evolution Reaction. *J. Mater. Chem. A* **2019**, *7* (44), 25593–25608.

(225) Lv, L.; Yang, Z.; Chen, K.; Wang, C.; Xiong, Y. 2D Layered Double Hydroxides for Oxygen Evolution Reaction: From Fundamental Design to Application. *Advanced Energy Materials*. 2019, p 1803358.

(226) Qin, M.; Li, S.; Zhao, Y.; Lao, C. Y.; Zhang, Z.; Liu, L.; Fang, F.; Wu, H.; Jia, B.; Liu, Z.; Wang, W. (Alex); Liu, Y.; Qu, X. Unprecedented Synthesis of Holey 2D Layered Double Hydroxide Nanomesh for Enhanced Oxygen Evolution. *Adv. Energy Mater.* **2019**, *9* (1), 1803060.

(227) Yang, H. Bin; Miao, J.; Hung, S.-F.; Chen, J.; Tao, H. B.; Wang, X.; Zhang, L.; Chen, R.; Gao, J.; Chen, H. M.; Dai, L.; Liu, B. Identification of Catalytic Sites for Oxygen Reduction and Oxygen Evolution in N-Doped Graphene Materials: Development of Highly Efficient Metal-Free Bifunctional Electrocatalyst. *Sci. Adv.* **2016**, *2* (4), e1501122.

(228) Chai, G. L.; Qiu, K.; Qiao, M.; Titirici, M. M.; Shang, C.; Guo, Z. Active Sites Engineering Leads to Exceptional ORR and OER Bifunctionality in P,N Co-Doped Graphene Frameworks. *Energy Environ. Sci.* **2017**, *10* (5), 1186–1195.

(229) Najafi, L.; Bellani, S.; Castelli, A.; Arciniegas, M. P.; Brescia, R.; Oropesa-Nuñez, R.; Martín-García, B.; Serri, M.; Drago, F.; Manna, L.; Bonaccorso, F. Octapod-Shaped CdSe Nanocrystals Hosting Pt with High Mass Activity for the Hydrogen Evolution Reaction. *Chem. Mater.* **2020**, *32* (6), 2420–2429.

Germanium selenide (GeSe) nanoflakes are produced through liquid-phase exfoliation to be directly used for photoelectrochemical-type photodetectors and photoelectrochemical water splitting

Photoelectrochemistry

Gabriele Bianca, Marilena Isabella Zappia, Sebastiano Bellani, Zdeněk Sofer, Michele Serri, Leyla Najafi, Reinier Oropesa-Nuñez, Beatriz Martín-García, Tomáš Hartman, Luca Leoncino, David Sedmidubský, Vittorio Pellegrini, Gennaro Chiarello and Francesco Bonaccorso

Liquid-phase exfoliated GeSe nanoflakes for photoelectrochemical-type photodetectors and photoelectrochemical water splitting